SIXTH TECHNICAL PROGRESS REPORT

ON

HYDRODYNAMIC MODELS FOR SLURRY BUBBLE COLUMN REACTORS

JANUARY 1996

U.S. DEPARTMENT OF ENERGY GRANT
DE-FG22-94PC94208

DIMITRI GIDASPOW
PRINCIPAL INVESTIGATOR
DEPARTMENT OF CHEMICAL AND ENVIRONMENTAL ENGINEERING
ILLINOIS INSTITUTE OF TECHNOLOGY
CHICAGO , ILLINOIS 60616

U.S. DOE PATENT CLEARANCE NOT REQUIRED PRIOR
TO PUBLICATION OF THIS REPORT

DISCLAIMER

ABSTRACT

HYDRODYNAMIC MODELS FOR SLURRY BUBBLE COLUMN REACTORS

The objective of this investigation is to convert our "learning gas - solid - liquid" fluidization model into a predictive design model . The IIT hydrodynamic model computes the phase velocities and the volume fractions of gas , liquid and particulate phases . Model verification involves a comparison of these computed velocities and volume fractions to experimental values .

As promised in the FIFTH TECHNICAL PROGRESS REPORT , October 1995 , this report presents our measurements of granular temperature of Air Products catalyst . The report is in the form of a preliminary paper , entitled " Dynamics of Liquid - Solid Fluidized Beds with Small Catalyst Particles " . The principal results are as follows :

1- For the liquid - solid system the granular temperature is much smaller than for a corresponding gas - solid system , as reported by Gidaspow and Huilin at the November 1995 AIChE meeting in Miami Beach .
This may be due to the larger viscosity of the liquid in comparison to air .
2- The collisional viscosity of the catalyst is correspondingly much smaller than that of catalyst particles in the air .
3- The dominant frequency of density oscillations is near two Hertz , as expected for a gas - solid fluidized bed . There exists a link between this low frequency and the high frequency of catalyst particle oscillations .

For the next quarter we plan to conduct similar experiments in our apparatus that is a rough approximation of the Air Products system that we modeled . We need data for granular temperature as a function of gas flow rates to see whether our " guessed " (computed) granular temperatures in the simulation were realistic .

We strongly urge Air Products to measure the granular temperature in their reactor . This can be done using the EXXON acceleration probe , as described by Dr . CODY (Fluidization and Fluid - Particle Systems Preprints , AIChE Annual Meeting , 1995 , pages 96-100) at the Miami Beach meeting .

BED DESIGN FOR A 2 DIMENSIONAL THREE - PHASE BED WITH MULTIPLE JET INLETS

To simulate a slice of the Air Products methanol reactor with jets a thin rectangular three phase fluidized bed was designed and constructed . Symmetry is achieved by controlling the gas at multiple inlets .

In order to have a symmetric system seven identical jets $7/8 \times 7/8 \times 3$ inches are installed at the bottom of the bed . See Fig A below . Each of these jets is connected to a valve to control the gas flow rates . The reason for using square jets is to eliminate the 3D effects caused by circular jets. At the bottom of each jet a cloth type material (with a pressure drop of 2 psi at the maximum gas flow rate) is used to prevent the $50\ \mu m$ catalyst particles from going inside the gas pipe . The bed is constructed of $1/2$ inch thickness Plexiglas . An opening at the top of the bed lets the air go out of the bed to the atmosphere . See Fig B .

The air flow rate can be varied up to 190 cf/hr at a pressure of 40 psi in order to achieve a superficial gas velocity of 12 cm/sec .In a typical Air Products experiment the weight ratio of solid to liquid was about 2:3 .The dimensions of the bed are given in the figure.

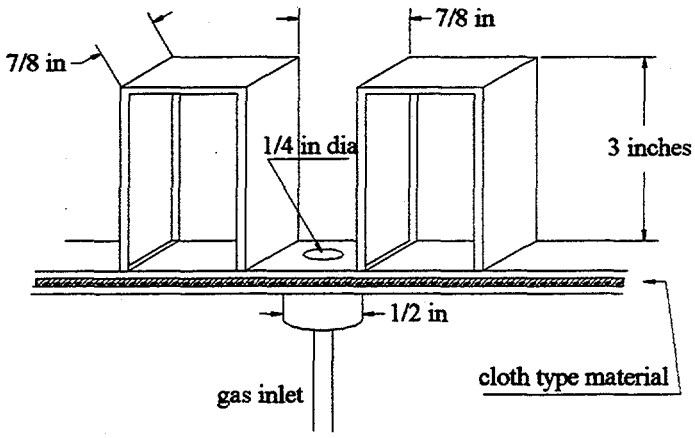

Fig A - JET DETAILS

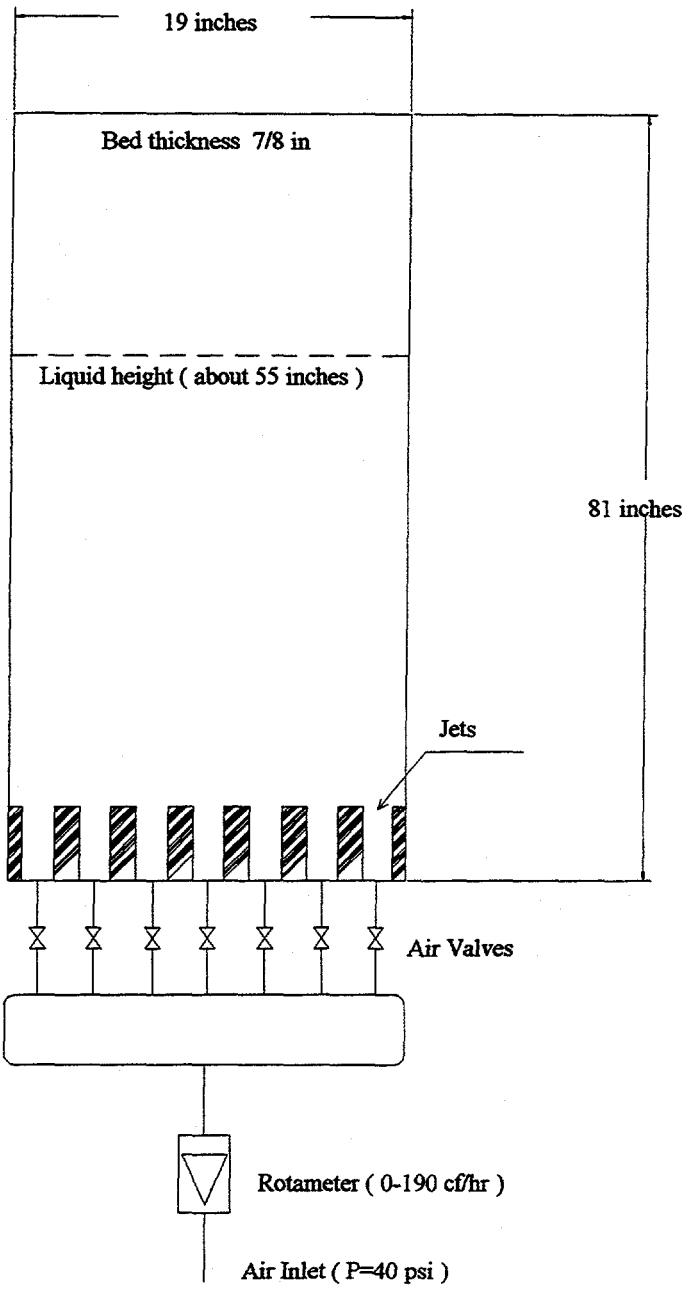

Fig B - SKETCH OF THREE - PHASE FLUIDIZED BED FOR MEASUREMENTS OF GRANULAR TEMPERATURE (TURBULENCE) APPROACHING AIR PRODUCTS METHANOL SYNTHESIS REACTOR WITH NO LIQUID FLOW

Dynamics of Liquid-Solid Fluidized Beds With Small Catalyst Particles

Principal Investigator: Dimitri Gidaspow
Research Assistant: Lu Huilin

Department of Chemical and Environmental Engineering
Illinois Institute of Technology
Chicago, Il. 60616

Introduction

This study is part of a larger effort to understand the dynamics of three phase fluidized bed reactors containing catalyst particles. Such reactors, as reviewed by Fan (1989) are used in a variety of industrial applications. The present interest is in slurry bubble column reactors that are being developed by Air Products and Chemicals under a U. S. Department of Energy sponsorship to produce methanol and synthetic fuels from synthesis gas. Slurry flow was recently reviewed by Shook and Roco (1991). Liquid-solid fluidized beds are of fundamental interest due to absence of complications caused by formation of bubbles in three phase systems. A brief review of some basic studies is as follows :

Carlos and Richardson (1968), using a photographic method, examined the particle velocity distributions in a liquid-solid fluidized bed. They found that the axial velocities greatly exceeded the radial velocities, and that the experimental particle velocity distribution agreed with that predicted by the Maxwellian distribution. Fan et al. (1985), using a still camera and a high-speed movie camera, found that the particle velocity increases linearly with the liquid velocity in two-dimensional liquid-solid fluidized beds. Poze et al. (1993), using a new technique of a tethered particle, detected the particle-particle collisions in liquid-solid fluidized beds. They found that the collision frequency was a maximum at minimum fluidization, and that it decreased with increasing liquid velocity. Larachi et al. (1995), using a non-invasive gamma-ray emission particle tracking technique, examined the motion of large particles in a liquid-solid fluidized bed containing a binary mixture of solids. They found that turbulence or dispersive motion dominates the radial solids transport, and that turbulent transport is anisotropic with higher axial than radial velocities. Anderson and Jackson (1961), using an optical technique, measured the characteristic wavelength and the speed of propagation in liquid-solid fluidized beds. Bahary (1994) and Gidaspow et al. (1995), using a CCD camera technique, determined particle velocity distributions in liquid-solid and liquid-solid-gas fluidized beds. The granular temperature was obtained from particle velocities distributions for two flow rates for 800 μm particles.

In the above studies, the solid volume fractions were usually obtained from the expanded bed height which was determined from either visual observations or from the static pressure profile. These average solid volume fractions are insufficient to describe the

local hydrodynamics of the bed. Fan et al. (1985) determined solid volume fractions by means of the counting of the number of particles present in a unit volume on still photographs. Gidaspow et al. (1995), using an x-ray densitometer, measured local solid volume fractions in liquid-solid fluidized beds. Daly et al. (1995), using a gamma ray densitometer, measured local phases volume fractions in three-phase bubble columns. Turner (1973), a using conductivity technique, measured the electrical conductivity of fluidized beds of ion-exchange resin beads, fluidized by aqueous solutions of different conductivities in liquid-solid fluidized bed. Begovich et al. (1978), using an electroconductivity technique, measured the distribution of solid concentration in the three phase fluidized beds. They found that the electroconductivity technique can be used for determining the overall phase concentrations or local phase concentrations in three phase fluidized beds as a function of height of column. Galy-Jammou et al. (1995), using the conductivity technique, correlated the conductivity readings to the corresponding volume fraction of phases in three-phase fluidized beds. Their conductivity probe was calibrated in the liquid-solid fluidized bed, and solid volume fraction was obtained from the known mass of solids in the bed and expanded bed height which was visually measured.

The first objective in this paper was, therefore, to develop an accurate method of measuring local solid volume fractions in the solid-liquid fluidized bed which could be applied to any kind of particle-liquid system. Using a CCD camera system, particle velocity distributions were measured. The second objective was to obtain solid viscosity, solid sonic velocity and particle collision frequency based on the kinetic theory.

Fluidization Equipment

A two-dimensional bed was used as the fluidization unit, see Figure 1. Its total height was 1.85 m, with a 1.2 m high test section. The cross-section was 30.48 cm by 5.08 cm. A centrifugal pump was connected to the bottom of the bed by a 2.54 cm I.D. stainless steel pipe. The flowrate of liquid, water, was regulated and measured using a calibrated rotameter. Good liquid distribution was obtained with the help of a pipe distributor containing 42 holes (d=4 mm), and a perforated plate. Water was circulated through a surge tank. A plastic grid was attached to the top of the bed to minimize the entrainement of particles by water. The particles were fed into the bed by means of a screw feeder placed on top of the bed to maintain constant solid weight in the bed.

Copper oxide catalyst particles with an average diameter of 50 μm and a density of 1300 kg/m^3 were used as the solid phase. Unfluidized bed height of particles was 20 cm from the perforated distributor. Local solid volume fractions were measured by means of a conductivity probe. The particle velocities were determined using the high resolution micro-imaging/ measuring system (Gidaspow et al., 1995).

Particle Velocity Determination

The High Resolution Micro-Imaging/Measuring System for the particle velocity measurements consists essentially of two units: a high resolution micro-image system and a

data managing system. See Fig. 1. The high resolution micro-image system is a 2/3 inch color video camera (DXC-151A) which uses a Charge Coupled Device (CCD), a solid stage image sensor. This camera has ten electronic shutter settings and four modes for gain control. The horizontal resolution of the camera is 460 TV line, and a sensitivity of 2000 lux at 0 dB for gain. The camera adaptor is a Sony CMA-D2 which connects the camera to a 486/33 MHz IBM computer. The personal computer has a Micro-Imaging Board and a Micro-imaging software, Image-Pro Plus, for data measurement and analysis. Bahary (1994) demonstrated this technique for gas-liquid-solid fluidization (Gidaspow et al., 1995).

For good visualization of microscopic movement of particles, a fiber-optic light was used. The area of view in most experiments was a 5×20 mm. As the particles were fluidized inside the bed, the camera with a zoom lens, 18-108 mm and close up focus transferred its field of view into the monitor. Fig. 2 shows a typical streak made by the particles. These streak lines represent the distance traveled by the particles in a given time interval specified on the camera. The images were then captured and digitized by the Image-Pro Plus software. To obtain reliable velocity information, the time between exposures must be selected so as to obtain a sufficient displacement to achieve an acceptable velocity resolution, but must not be so large that the particle moves out of the field of view. The local velocity is then estimated from equation:

$$u = \frac{\Delta L(x,y)}{\Delta t} \tag{1}$$

Two dimensional velocity components, radial and vertical are determined.

Particle Concentration Measurements

Local solid volume fraction measurements were performed with a conductivity technique. A pair of electrodes were placed at the center of the wall opposite each other at a height of 10 cm from the plate distributor. After investigating various materials, such as stainless steel and copper, brass was chosen as the most suitable material for the electrode. Successive tests determined the optimum shape of the electrodes to be a trapezoidal surface, 1.6 cm high and 1.1 and 1.3 cm wide. The small electrode thickness (1.0 mm) did not modify local hydrodynamics. The probe combining a copper-constant thermocouple connected into a 1481-00 conductivity meter (Cole-Parmer Instrument Company). It features 3 modes of operation: 2 for the measurement of conductivity in 5 different spans; and 1 for self-check and has an automatic temperature compensation in the range of $5 \sim 65$ ^{o}C. Its signal connects to a T31-B terminal (Strawberry Tree), and is sampled by an IBM PC computer with a data acquisition card ACAO mounted in the computer by a data acquisition software package called ACQ. Sampling frequency was at least 200 Hz with a sampling time of 30 seconds. This yielded the most reproducible and stable results.

A calibration of this conductivity probe was performed in the calibration container, see Fig. 3. For dispersed particles in a unit cube, the approach was to slice the unit cube, and to "collect" the dispersed particles into a strip, as in Figure 3. The conductivity of such strip would have the same value as the original system (Tsao, 1961; Cheng et al., 1969). It is necessary to calibrate this particle probe.

Two rectangular columns, a small one of 5.08×1.9×1.5 cm and a large one of 5.08× 4.5×20.5 cm, were constructed from the same material as the fluidized bed. Each column was immersed into a tank containing the same weight of water and particles as the fluidized bed. Knowing the weight of the particles added into the column, readings with conductivity meter were taken. Thus a relation with the solid volume fraction and conductance or voltage was determined. A calibration curve between the solid volume fraction and voltage from the conductivity meter was obtained. Figure 4 shows the results of calibration for two different sizes of column. This calibration was found to give a reasonable resolution when the solid volume fraction was greater than about 0.3 in this study. In this range, the results are similar to those given by the Maxwell equation.

Results and Discussion

Solid Volume Fraction Fluctuations

Solid volume fraction fluctuations with time are shown in Figures 5 a and b for liquid velocities of 0.77 cm/s and 1.65 cm/s, respectively. Time-averaged solid volume fractions corresponding to the liquid velocities were 0.5397 and 0.3989. A comparison of the two plots indicates that the amplitude of the solid volume fraction fluctuations at the lower liquid velocity is less than at the higher liquid velocity. The theory (Gidaspow, 1994, Eq 10.20) shows that this is due to the higher mean free path at the higher (more dilute) flow .

Figures 6 a and b illustrate the probability distributions of solid volume fraction fluctuations for liquid velocities of 0.77 and 1.65 cm/s, respectively. The area under each curve is equal to unity. The variances of solid volume fractions are 0.020 and 0.055, respectively. Figure 7 shows the variance of solid volume fraction fluctuations in this study. This plot reveals that a maximum variance exists at a liquid velocity corresponding to a solid volume fraction about 0.4. This finding is consistent with that of Fan et al. (1985) who obtained maximum of variances of about 0.33 to 0.20.

Figures 8 a and b show the power spectrum density of solid volume fraction fluctuations at liquid velocities of 0.77 and 1.65 cm/s, respectively. It is clear that a strongly dominant peak emerges at the lower liquid velocity. Several peaks appear at the higher liquid velocity, although a dominant frequency can still be distinguished. Figure 9 shows the dominant frequency as a function of solid volume fraction. The dominant frequency increases with an increasing liquid velocity (Anderson and Jackson, 1969; Didwania et al., 1981, Poletto et al., 1995).

Particle Velocity Distributions and Granular Temperature

Typical particle speed, axial and radial velocity distributions are shown in Figures 10 and 11 a, b and c for liquid velocities of 0.77 and 1.65 cm/s, respectively. The ordinate is the probability that the velocity will fall in the indicated velocity range. It is obtained by dividing the number of particles in the velocity range shown by the total number of measurements

and by the velocity in the indicated velocity range. The area under the distribution is unity. The shape of the curves are very similar to the Carlos and Richardson (1968) and Fan et al. (1985) studies. Anisotropy in the velocity distributions has been observed previously (Handly et al., 1966; Carlos and Richardson, 1968)

Average particle speed, axial and radial velocities are plotted versus liquid velocity in Figures 12 and 13. The figures illustrate that each velocity component increases as the liquid velocity increases (Fan et. al., 1985), and that the axial velocities are greater than radial velocities. The ratio of the root mean square of the axial to radial velocities is about 2.1. This value is very close to the value of 2.16 reported by Latif et al. (1972) and 2.3 by Handly et al. (1966). Fig 12 also shows that there is average positive slip between the particles and the fluid , as expected in a fluidized bed .

The standard deviations were calculated based on instantaneous velocity of particles from mean values:

$$\sigma = \frac{1}{N}\sum_{i=1}^{N}\sqrt{(u_i - u_m)^2} \tag{2}$$

where u_i and u_m are instantaneous and mean particle velocity, respectively. The mean particle velocity and speed are calculated as the arithmetic average. Shao et al. (1995) have used a similar procedure to calculate the fluctuating velocity using a laser dopper anemometer.

The granular temperature in kinetic theory as originally defined by Savage (1983) is one third the sum of the deviations of particle oscillations in the three directions. For isotropic flow all the three directions are equal and the granular temperature is simply the square of the velocity deviations, that is the random kinetic energy per unit mass. But data in table 1 show that the oscillations in the basic direction of flow called the x - direction are 20 to 100 % higher in the basic direction of flow. Since the CCD camera technique used did not permit a measurement of oscillation in third direction , between the plates of the bed, an assumption must be made for obtaining the granular temperature. Previously we assumed that there is isotropy in the non-basic directions of flow. This leads to the expression for granular temperature as :

$$\theta = \frac{1}{3}\left(\sigma_x^2 + \sigma_y^2 + \sigma_z^2\right) = \frac{1}{3}\sigma_x^2 + \frac{2}{3}\sigma_y^2 \tag{3}$$

To test the possible inaccuracy in this assumption, we recalculate the granular temperature assuming the standard deviation to be equal in the non-flow directions. This gives the formula for granular temperature as :

$$\theta = \frac{1}{2}\sigma_x^2 + \frac{1}{2}\sigma_y^2 \tag{4}$$

The granular temperature based on these methods is summarized in table 1. The differences are of the order of 20 % , not bad for the turbulence calculations .

Figure 14 shows the calculated granular temperature calculated used Eq. (3) as a function of solid volume fraction. The granular temperature increases with decreasing solid

volume fraction. This variation is consistent with data for flow of 75 μm FCC catalyst particles in a circulating fluidized bed for dense flow (Gidaspow and Huilin 1995). There in the dilute regime a maximum existed at about 10% of solid by volume. Experimental difficulties prevented us from obtaining data in the dilute regime for this system. For gas-solid flow the values of granular temperature were about one hundred times higher, probably due to larger drag and lower average velocities in this liquid - solid system. Handley et al. (1961) measured the trajectories of the tracer particles in a liquid-solid fluidized bed, and calculated the mean standard deviations of velocity components. Figure 15 shows a comparison of granular temperature variation with solid volume fraction for different particle diameters in liquid-solid fluidized beds.

Particulate Viscosity, Sonic Velocity and Particle Collision Frequency

Using kinetic theory of granular flow, one can calculate the solid viscosity in terms of particle properties, solid volume fraction and granular temperature. The following relationship for solid viscosity is given by Gidaspow (1994) based on the pioneering study of Lun, et al (1985):

$$\mu_s = \frac{5\rho_s d_p \sqrt{\pi\theta}}{48(1+e)g_o}\left[1+\frac{4}{5}(1+e)g_o\varepsilon_s\right]^2 + \frac{4}{5}\varepsilon_s^2\rho_s d_p(1+e)\left(\frac{\theta}{\pi}\right)^{0.5} \qquad (5)$$

where g_0 is the radial distribution function, and e restitution coefficient. A simple form for the radial distribution function g_0 is that used by Bagnold (1954), as reviewed by Gidaspow (1994):

$$g_o = \left[1-\left(\frac{\varepsilon_s}{\varepsilon_{s,\max}}\right)^{\frac{1}{3}}\right]^{-1} \qquad (6)$$

Figure 16 shows that the calculated solid viscosity as a function of solid volume fraction for different restitution coefficients. The solid viscosity increases with increasing solid volume fraction. The trend and the values of viscosity are similar to standard slurry viscosities (Shook and Roco, 1991) when one adds one centipoise to the solids viscosities in Fig. 16. This trend is same as for the gas-solid fluidized bed (Gidaspow et al., 1995)

A great many theoretical and empirical equations relating bed viscosity to solid concentration have been proposed (Darton, 1985; Shook and Roco, 1991, Fan L-S, 1989). Data from many different investigations of the viscosity of suspensions of particles were reported by Thomas (1965). These data were obtained with both rotational and capillary viscometers and represent a range of particle diameters from 0.099 to 0.435 microns. The particle materials included polystyrene, rubber latex, glass and methyl methacrlate. In all studies, either the density of the suspending medium was adjusted or the viscosity of the suspending medium was sufficiently large that settling was unimportant. An empirical equation of viscosity in terms of solid volume fraction was proposed. There was no particle size effect. Rigby et al (1970), using a Brookfield synchro-lectric viscometer, measured the apparent viscosity in a three phase fluidized bed with different particle sizes. They found the

particle size has only a minor effect on the viscosity of the bed. By measuring single gas bubble velocity, Darton and Harrison (1974) obtained the bed viscosity in a liquid-solid fluidized bed. They found that the bed viscosity decreases with increasing liquid velocity. It decreased with increasing particle size. Using a rotation viscometer, Michael et al. (1981) measured the apparent viscosity in liquid-solid fluidized beds. They found that the viscosity increases with increasing solid volume fraction. The viscosity measured with all these instruments reflects the viscosity of the fluid plus the viscosity shown in Fig 16.

Solid pressure as a function of solid properties, solid volume fraction and granular temperature is given as follows based on the work of Savage (1983) and co-workers (Gidaspow, 1994):

$$p_s = \rho_s \varepsilon_s \theta \left[1 + 2\varepsilon_s g_0 (1+e)\right] \tag{7}$$

Figure 17 shows the estimated solid pressure as a function of solid volume fraction for different restitution coefficients. Comparison of solid pressure data to that for gas-solid fluidized beds (Campbell and Wang, 1991; Chen et al., 1994), shows the values of solid pressure in liquid-solid fluidized bed to be smaller than that in gas-solid fluidized beds.

The pseudo-sonic velocity of particles is (Savage, 1988):

$$C_s = \sqrt{\frac{1}{\rho_s}\frac{\partial p_s}{\partial \varepsilon_s}} \tag{8}$$

Figure 18 shows the estimated particle sonic velocity as a function of solid volume fraction for different of restitution coefficients. It can be seen that particle sonic velocity decreases with decreasing solid volume fraction. This is agreement with the data of Anderson and Jackson (1969). Particle sonic velocity was found to be about 4.0 cm/s in liquid-solid fluidized beds (Jackson, 1985; Poletto et al., 1995).

Figure 19 shows the particle collision frequency as a function of solid volume fraction calculated according to following equation (Gidaspow, 1994):

$$f_{colli} = 6.77\left(\frac{\varepsilon_s}{d_p}\right) g_0 \sqrt{\theta} \tag{9}$$

It can be seen that the particle collision frequency increases with increasing solid volume fraction. We see that in liquid - solid fluidized beds similar to gas fluidized beds , as reviewed by Gidaspow (1994) there are two type of oscillations , the rapid ones caused by the particle collisions as depicted in Fig. 19 .and the low oscillations shown in Fig 9.

Figure 20 shows the variation of the dominant frequency with the characteristic velocity $\left|C_s - u_p\right|$ for liquid-solid fluidized beds, where u_p is average particle velocity. When the particle sonic velocity equals the average particle velocity, the frequency becomes zero. The plot in Fig. 20 comes from one dimensional Theory of characteristics for two phase flow (Gidaspow, 1994). Waves move with the velocity shown as the abscissa in Fig. 20. Such a relationship was previously found to hold for gas - solid flow in a vertical pipe (Gidaspow et al 1995). Fig. 19 gives an effective wave length of about 3.3 cm. The corresponding length for flow of 75 μm FCC particles in a circulating fluidized bed was

about 2 meters, roughly corresponding to the length of an annular particle region. Anderson and Jackson (1969), based on an instability analysis, had anticipated that in liquid - solid fluidized beds this wave length would be 100 times smaller than in the gas - solid beds. These experiments confirm their prediction .

REFERENCES:

Anderson T. B. and R. Jackson, A fluid mechanical description of fluidized beds: Comparison of theory and experiment, *Indust. Engng Chem. Fundls*, **8**, 137-144, 1969.

Bagnold R. A., Experiments on a gravity free dispersion of large solid spheres in a Newtonian fluid under shear, *Proc. Roe. Soc.*, **A255**, 49-63, 1954.

Bahary, M., Experimental and computational studies of hydrodynamcis in two and three phase fluidized beds, Ph. D. Thesis, IIT, 1994.

Begovich J. M. and J. S. Watson, An electroconductitvity technique for measurement of axial variation of holdups in three-phase fluidized beds, *AIChE J.*, **24**, 351-354, 1978.

Campbell C. S. and D. G. Wang, Particle pressure in gas fluidized beds, *J. Fluid Mech.*, **227**, 495-508, 1991.

Carlos C. R. and J. F. Richardson, Solid movement in liquid fluidized beds I: Particle velocity distribution, *Chem. Eng. Sci.*, **23**, 813-824, 1968.

Chen C. J., W. Polashenski and K. Tuzla, Normal solid stress in fluidized beds, AIChE Annual meeting, San Francisco, Nov. , 1994.

Cheng S. C. and R. I. Vachon, The prediction of the thermal conductivity of two and three phase solid heterogeneous mixtures, *Int. J. Heat Mass Transfer*, **12**, 249-264, 1969.

Daly J. G., S. A. Patel and D. B. Bukur, Measurement of gas holdups in a three phase bubble column by gamma ray densitometry, *Fluidization VIII*, Edited by C. Laguerie and J. F. Large, France, 417-424, 1995.

Darton R. C. and D. Harrison, The rise of single gas bubbles in liquid fluidized beds, *Trans. Instn. Chem. Engrs.*, **52**, 301-306, 1974.

Darton R. C., The physical behavior of three-phase fluidized beds, *Fluidization*, Edited by J. F. Davidson and D. Harrison, Academic Press, 1985.

Didwania A. K. and G. M. Homsy, Flow regimes and flow transitions in liquid fluidized beds, *Int. J. Multiphase Flow*, 7, 563-580, 1981.

Fan L. -S., Gas-liquid-solid fluidization engineering, Butterworths Publishers, 1989.

Fan L.-S, T. Kawamura, D. C. Chitester and R. M. Kornosky, Experimental observation of nonhomogeneity in a liquid-solid fluidized bed of Small particles, *Chem. Eng. Commun.*, **37**, 141-157. 1985.

Galy-Jammou P., C. Briens, M. Bergougnou and J. F. Large, Local phase holdups in three-phase fluidized beds using a technique based on conductivity measurements, *Fluidization VIII*, Edited by C. Laguerie and J. F. Large, France, 375-382, 1995.

Gidaspow D. and L. Huilin, Collisional viscosity of FCC particles in a CFB, 1995 Annual Meeting of The America Institute of Chemical Engineers, Preprint Volume for Fluidization and Fluid-Particle Systems, Nov. 12-17, Miami Beach, 91-95, 1995.

Gidaspow, D., M. Bahary and Y. Wu, Slurry bubble column reactor models using kinetic theory, 1995 Annual Meeting of The America Institute of Chemical Engineers, Preprint Volume for Fluidization and Fluid-Particle Systems, Nov. 12-17, Miami Beach, 164-168, 1995.

Gidaspow D, Multiphase flow and fluidization: Continuum and kinetic theory descriptions, Academic Press, 1994.

Handley D. , A. Doraisamy, K. L. Butcher, N. L. Franklin, A study of the fluid and particle mechanics in liquid-fluidized beds, *Trans. Instn. Chem. Engrs*, **44**, 260-273, 1966.

Homsy G. M., M. M. El-Kaissy, A. K. Didwania, Instability waves and the origin of bubbles in fluidized beds-II Comparison of theory with experiment, *Int. J. Multiphase Flow*. **6**, 305-318, 1980.

Jackson R., Hydrodynamic stability of fluid-particle systems, *Fluidization*, Edited by J. F. Davidson and D. Harrison, Academic Press, 1985.

Larachi F., E. Lord, J. Chaouki, C. Chavarie and L. A. Behie, Phenomenological study of solids mixing in a binary liquid fluidized bed, *Fluidization VIII*, Edited by C. Laguerie and J. F. Large, France, 201-208, 1995.

Latif B. A. and J. F. Richardson, Circulation patterns and velocity distributions for particles in a liquid fluidized bed, *Chem. Eng. Sci.*, **27**, 1933-1949, 1972.

Michael R. and K. H. Reichert, Heat transfer of polythylene-hydrocarbon dispersions in bubble column reactors, *The Canadian J. Chemical Engineering*, **59**, 602-605, 1981.

Pozo M. D, C. L. Briens and G. Wild, Particle-particle collisions in liquid-solid and gas-liquid-solid fluidized beds, *Chem. Eng. Sci.*, **48**, 3313-3319. 1993.

Poletto M., R. Bai and D. D. Joseph, Propagation of voidage waves in a two-dimensional liquid-fluidized bed, *Int. J. Multiphase Flow*, **21**, 223-239, 1995.

Rigby G. R., P. Van Blockland, W. H. Park and C. E. Capes, Properties of bubbles in three phase fluidized beds as measured by an electroresistivity probe, *Chem. Eng. Sci.*, **25**, 1729-1741, 1970.

Savage S. B., Streaming motions in a bed of vibrationally fluidized dry granular material, *J. Fluid Mech.*, **194**, 457-478, 1988.

Shao S., H. J. Slovik and H. Arastoopour, The flight time technique for simultaneous measurements of particle flow parameters using a laser doppler anemometer (LDA), *Fluidization VIII*, Edited by C. Laguerie and J. F. Large, France, 201-208, 1995.

Shook C. A. and M. C. Roco, Slurry flow: Principles and practice, Butterworth-Heinemann, 1991.

Thomas D. G., Transport characteristics of suspension: VIII. A note on the viscosity of newtonian suspensions of uniform spherical particles, *J. Colloid Sci.*, **20**, 267-277, 1965.

Tsao G. T., Thermal conductivity of two-phase materials, *Ind. Engng. Chem.*, **53**, 395-397, 1961.

Turner J. C. R., Electrical conductivity of liquid fluidized beds, *AIChE Symposium Series*, **69**, 115-122, 1973.

Volpicelli G., Massimilla L. and Zenz F. A., Nonhomogeneities in solid-liquid fluidization, *Chemical Engineering Progress Symposium Series*, **42**, 42-50, 1966.

Table 1 Summary of Experimental Data

u_l cm/s	ε_s	$u_{p,av}$ cm/s	σ_y cm/s	σ_x cm/s	θ (cm/s)^2 Eq. (3)	θ (cm/s)^2 Eq. (4)
0.55	0.5917	0.4498	0.2118	0.2621	0.0528	0.056
0.77	0.5397	0.6199	0.2938	0.3891	0.1080	0.118
0.89	0.5076	0.7318	0.3770	0.5659	0.2015	0.231
1.11	0.4814	0.7851	0.3365	0.7632	0.2696	0.347
1.34	0.4471	0.9516	0.3438	0.8812	0.3376	0.447
1.54	0.4320	1.0490	0.4858	0.9315	0.4466	0.551
1.65	0.3989	1.0191	0.4811	1.1161	0.5695	0.738
1.76	0.3569	1.4564	0.5718	1.4239	0.8938	1.177
1.87	0.3525	1.4638	0.7581	1.4151	1.0506	1.288
1.98	0.3496	1.4814	0.8195	1.5111	1.2089	1.477

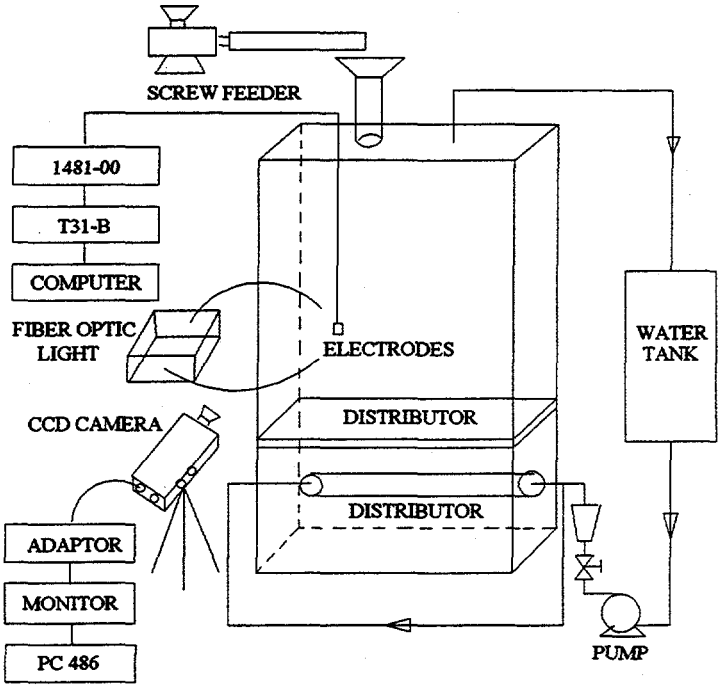

Fig. 1 Two-Dimensional Liquid-Solid Fluidized Bed With Instruments for Particle Velocity and Concenration Measurements

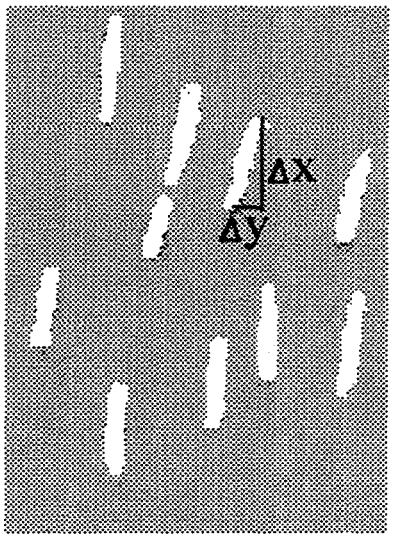

Fig. 2 Streak Images Captured by The CCD Camera Recording System For Flow of 50 μm Catalyst Particles in The IIT Liquid-Solid Fluidized Bed

(This figure shows a small portion from screen on which images are captured) (e.g.; Δx = 0.2595 mm; Δy = 0.1046 mm; Δt = 0.004 sec. Velocity is negative when streak is formed moving down on the computer monitor)

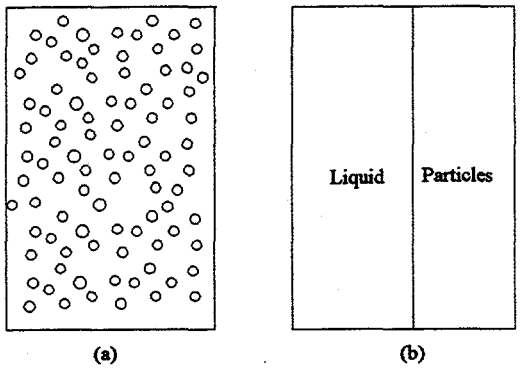

Fig. 3 Schematic of Calibration Container (a) A Slice of a Dispersion of Particles. (b) The Same Slice, With The Particles "Collected"

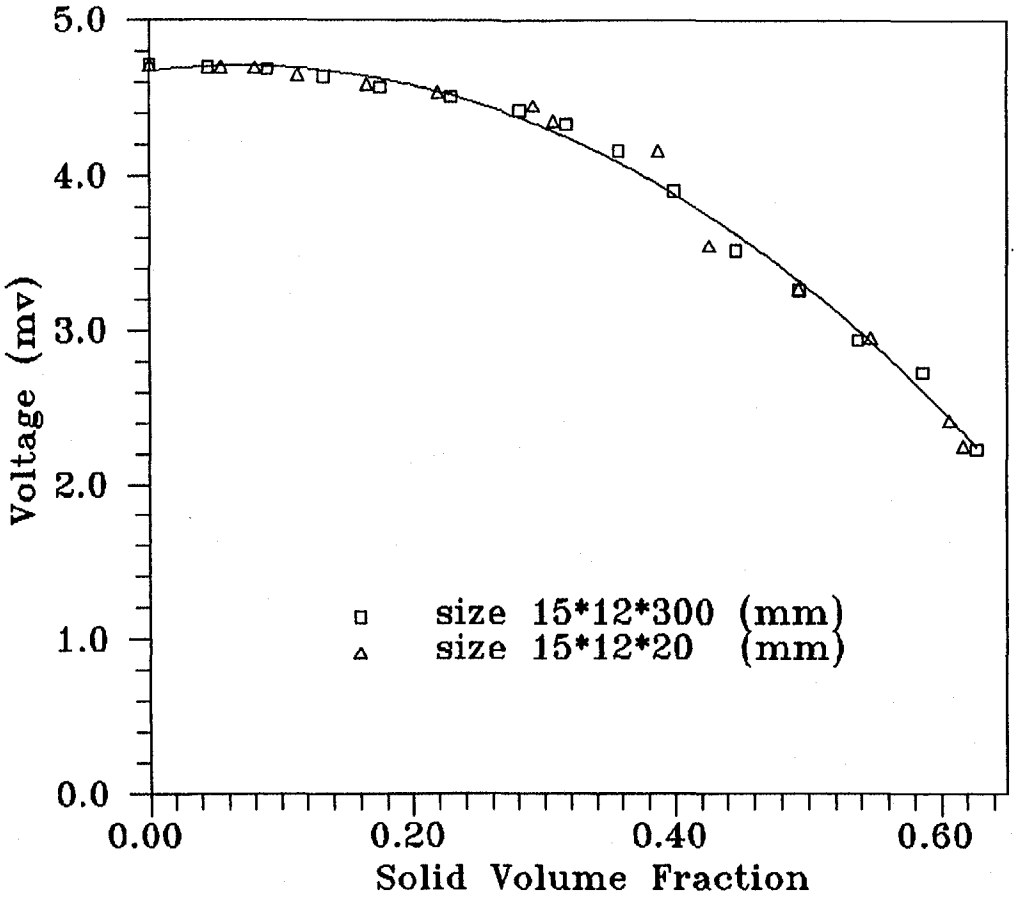

Fig. 4 Calibration Curve of Conductivity Probe

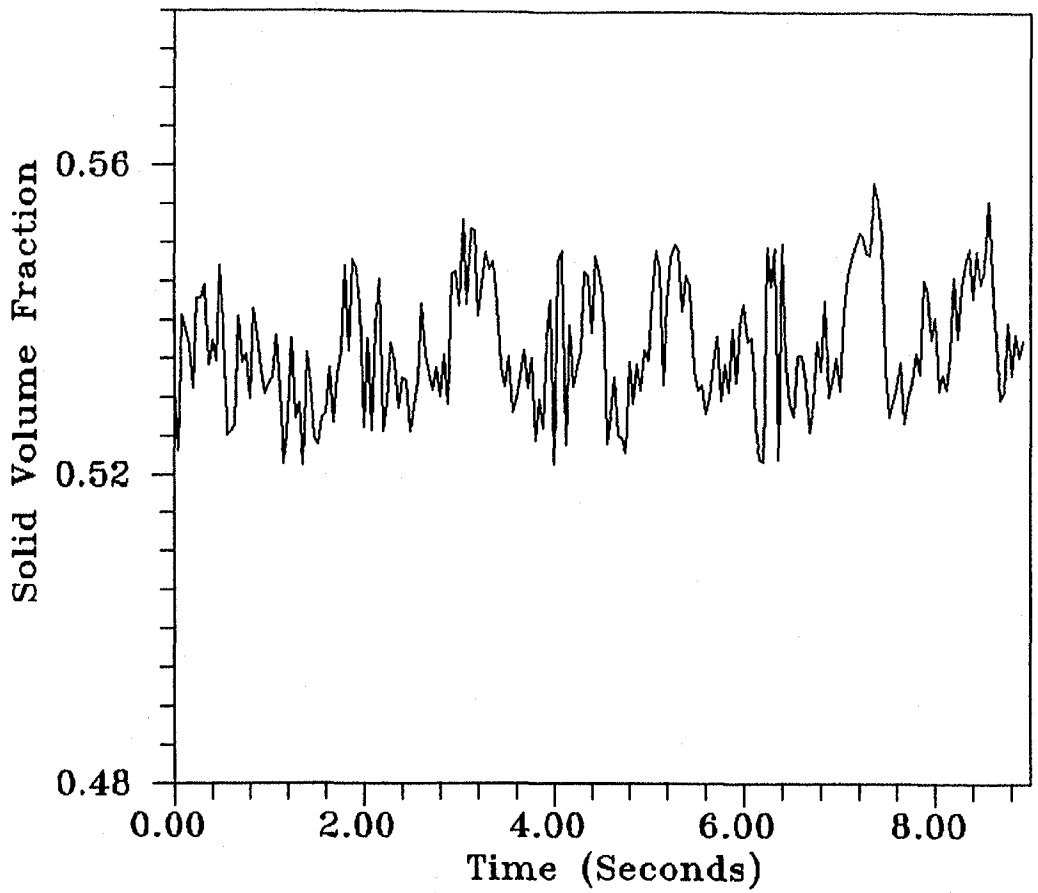

Fig. 5_a Instantaneous Solid Volume Fraction Variation For A Low Flow (U_l=0.77 cm/s)

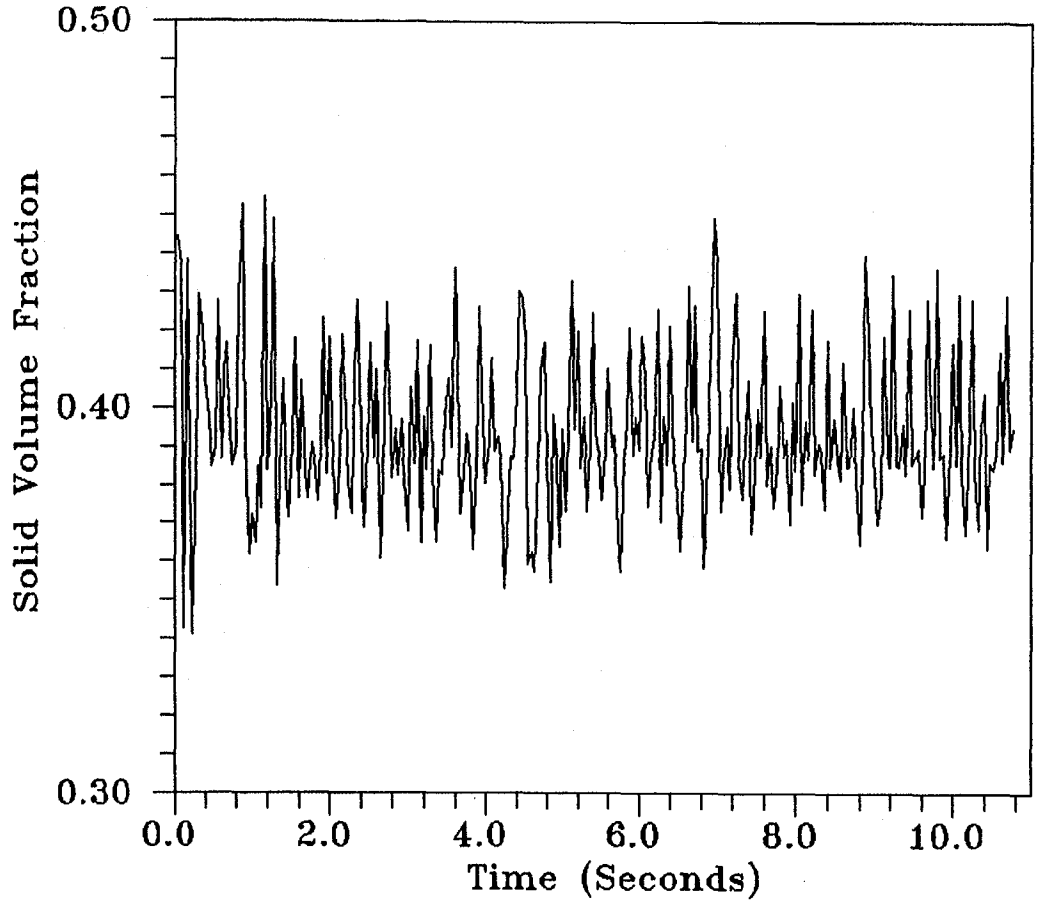

Fig. 5_b Instantaneous Solid Volume Fraction Variation For A High Flow (U_l=1.65 cm/s)

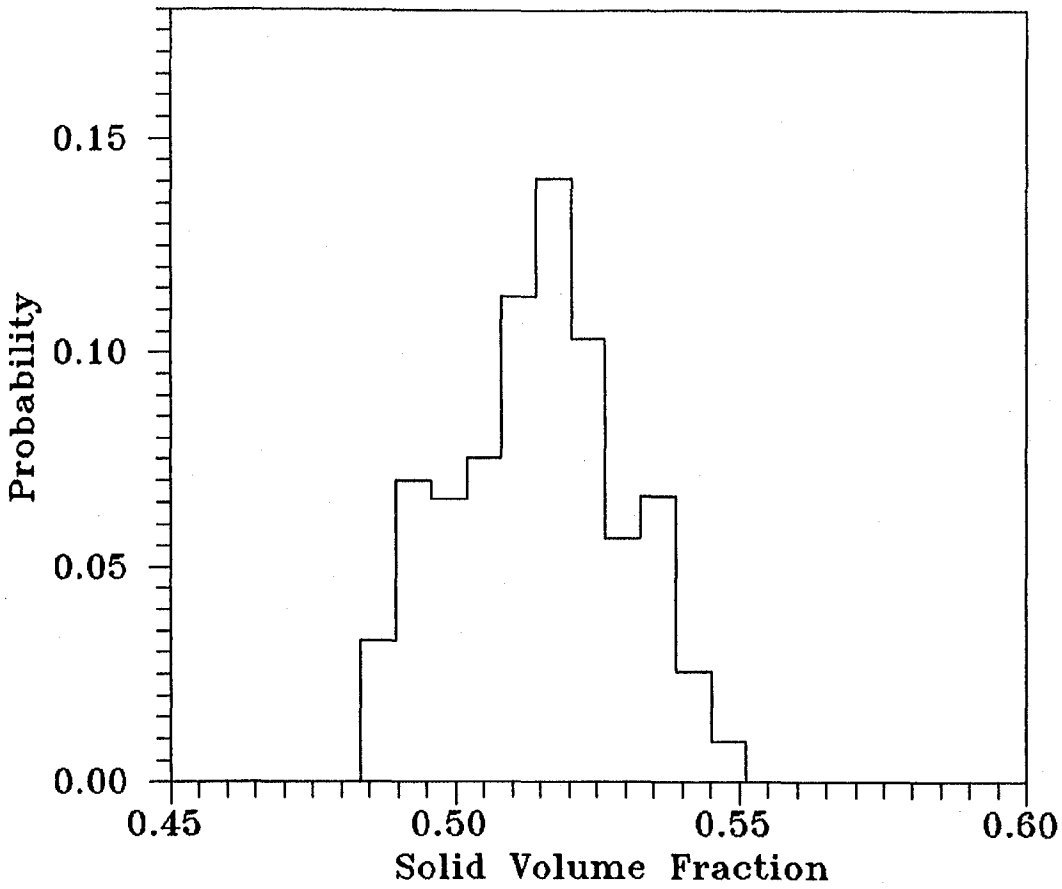

Fig. 6_a Distribution of Local Solid Volume Fraction At A Low Flow Rate (Mean Value=0.5397, Variance=0.02003, U_l=0.77 cm/s)

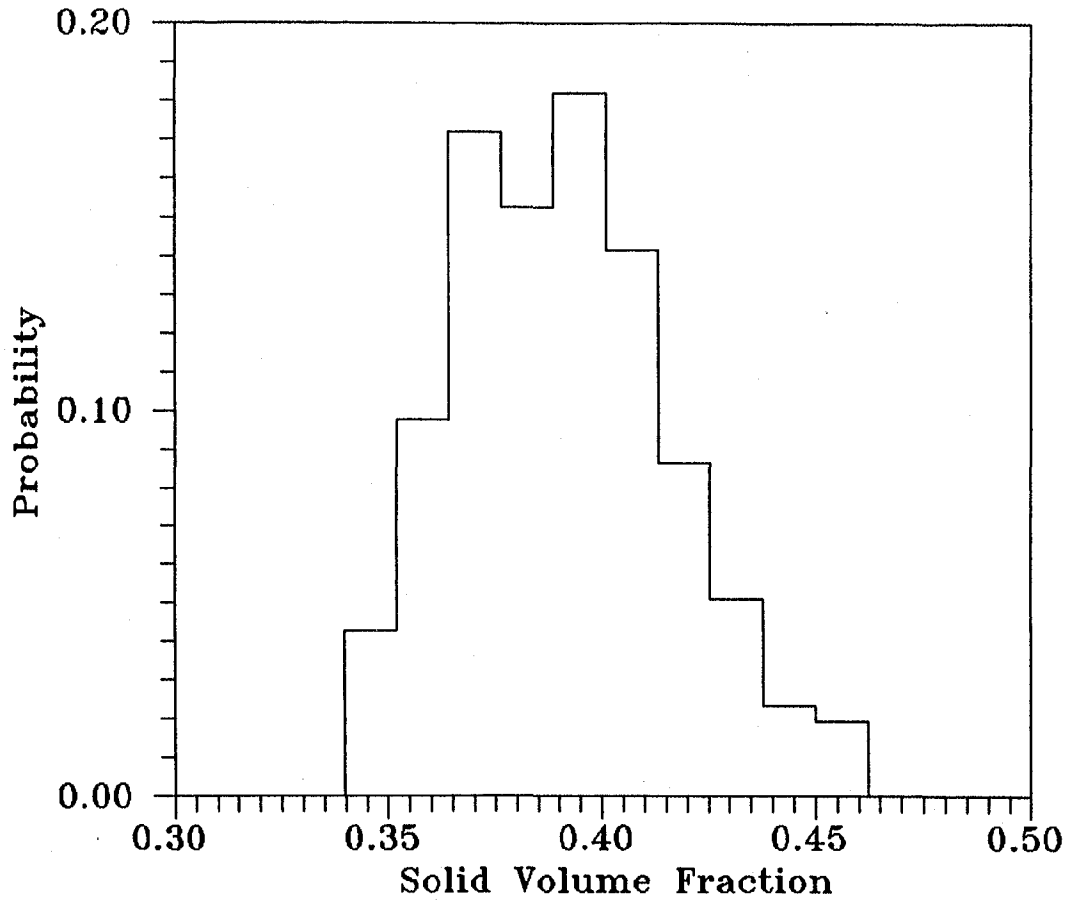

Fig. 6_b Distribution of Local Solid Volume Fraction At A High Flow Rate (Mean Value=0.3989, Variance=0.05515, U_l=1.65 cm/s)

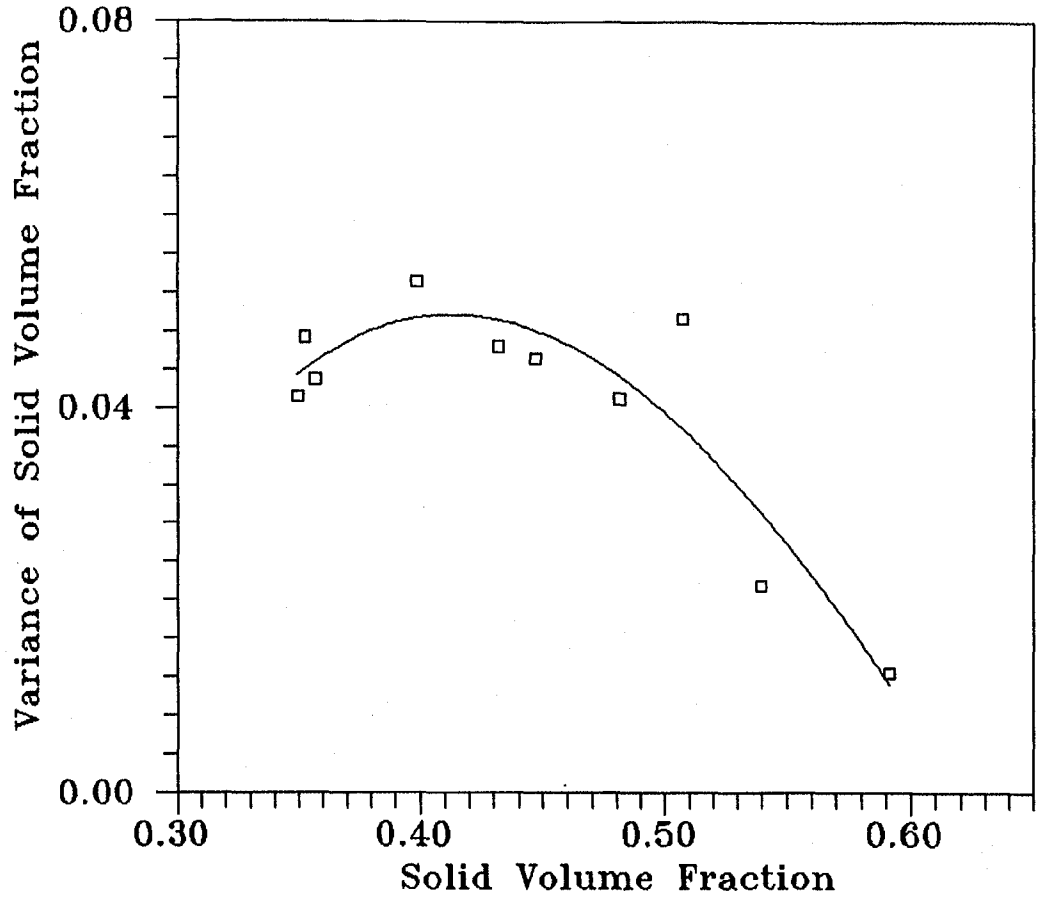

Fig. 7 Variance of Solid Volume Fraction for 50 Micron Catalyst Particles

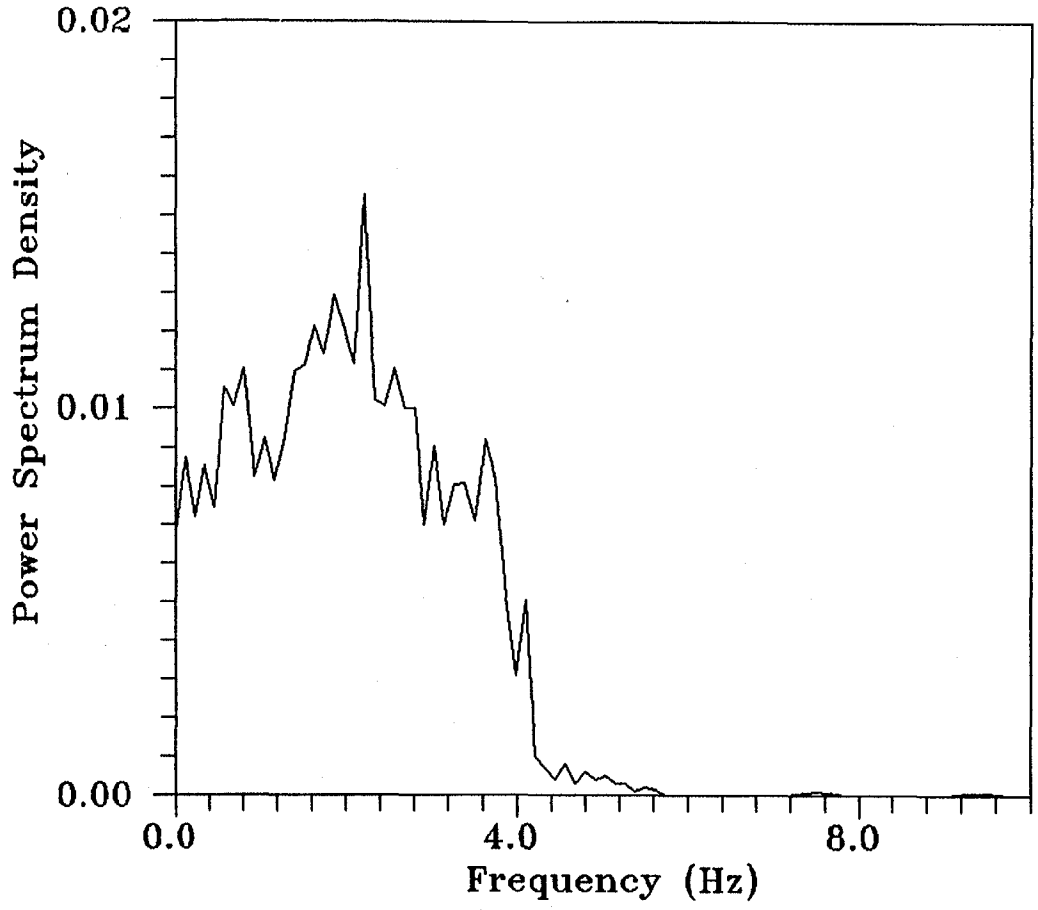

Fig. 8_a Power Spectrum Density of Solid Volume Fractions at A Liquid Velocity of 0.77 cm/s (Dominent Fequency = 2.2266 Hz)

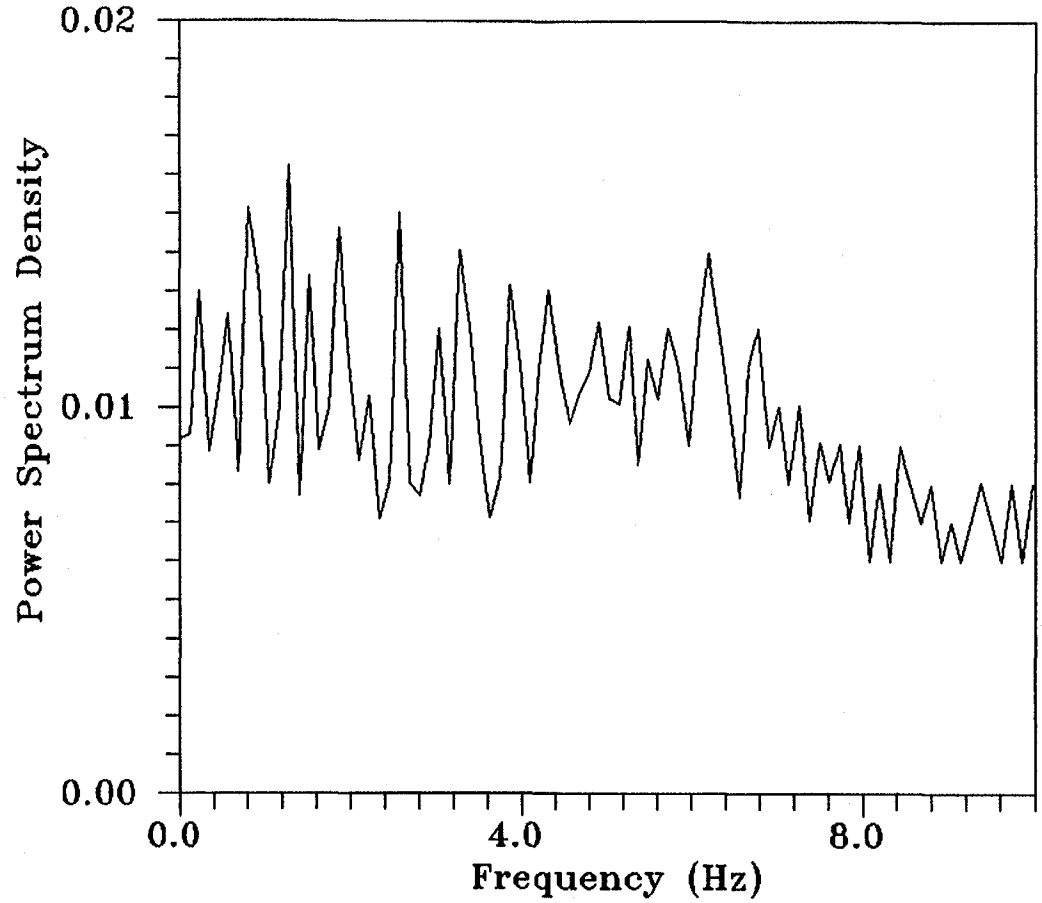

Fig. 8_b Power Spectrum Density of Solid Volume Fraction at A Liquid Velocity of 1.65 cm/s (Dominent Fequency = 1.2891 Hz)

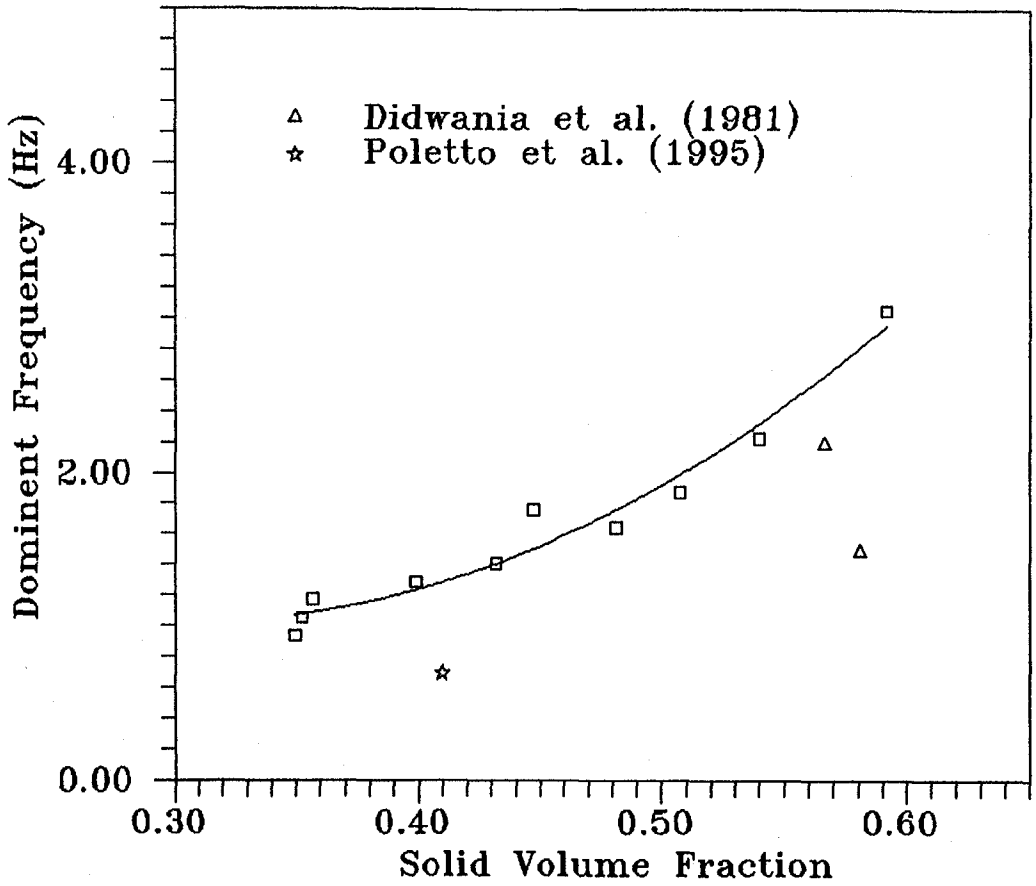

Fig. 9 Dominent Frequency of Volume Fractions For 50 Micron Catalyst Particles In A Liquid–Solid Fluidized Bed

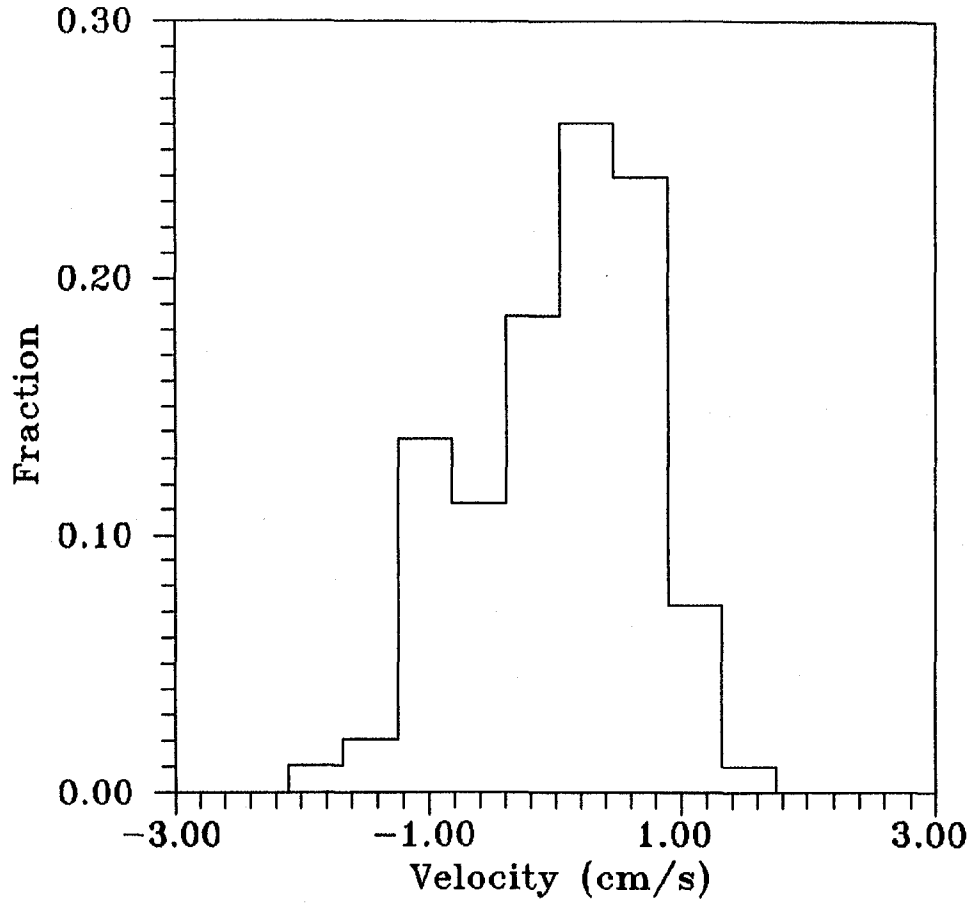

Fig. 10_a Particle Speed Distribution at Liquid Velocity=0.77 cm/s (Mean Value= 0.2177cm/s, Standard Deviation=0.515cm/s)

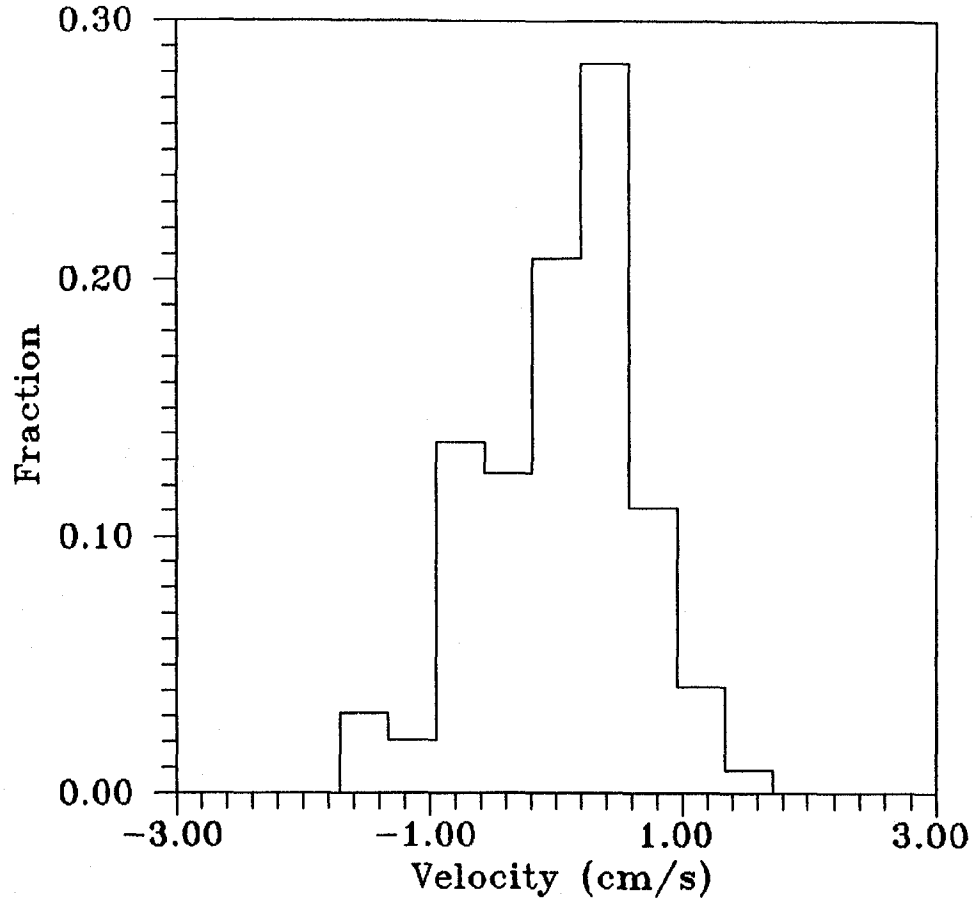

Fig. 10_b Particle Axial Velocity Distribution at Liquid Velocity=0.77 cm/s (Mean Value= 0.1959cm/s, Standard Deviation=0.389cm/s)

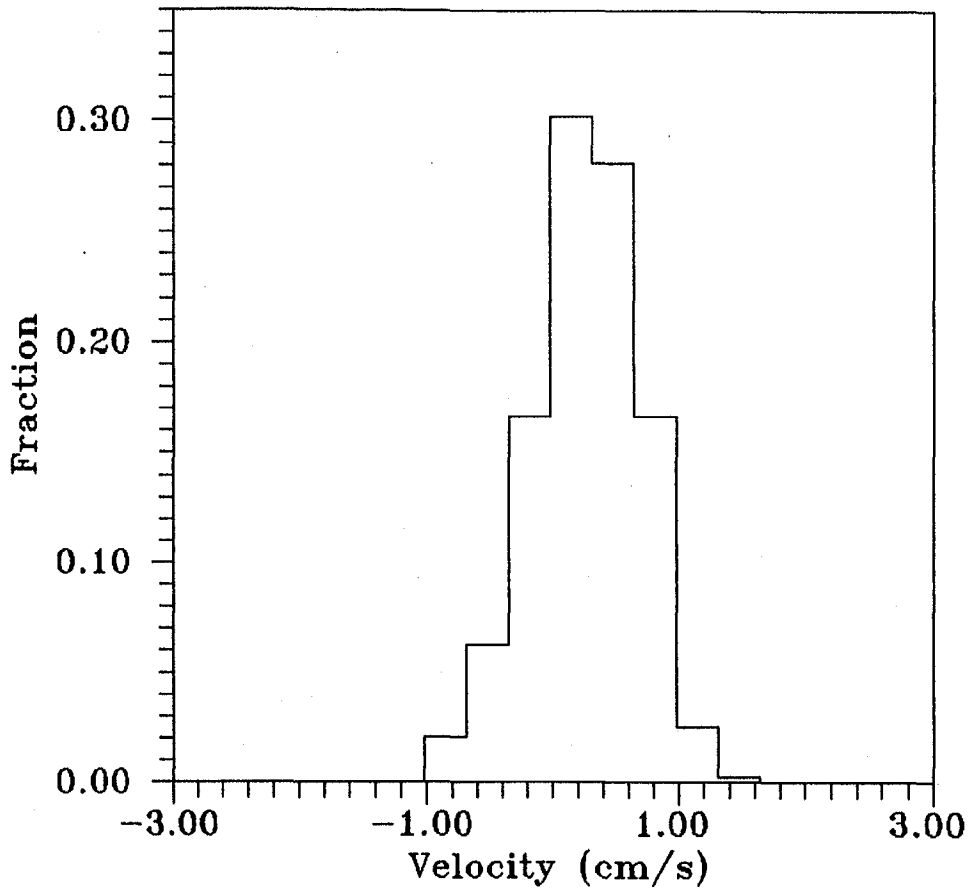

Fig. 10_c Particle Radial Velocity Distribution at Liquid Velocity=0.77 cm/s (Mean Value= 0.0692cm/s, Standard Deviation=0.2938cm/s)

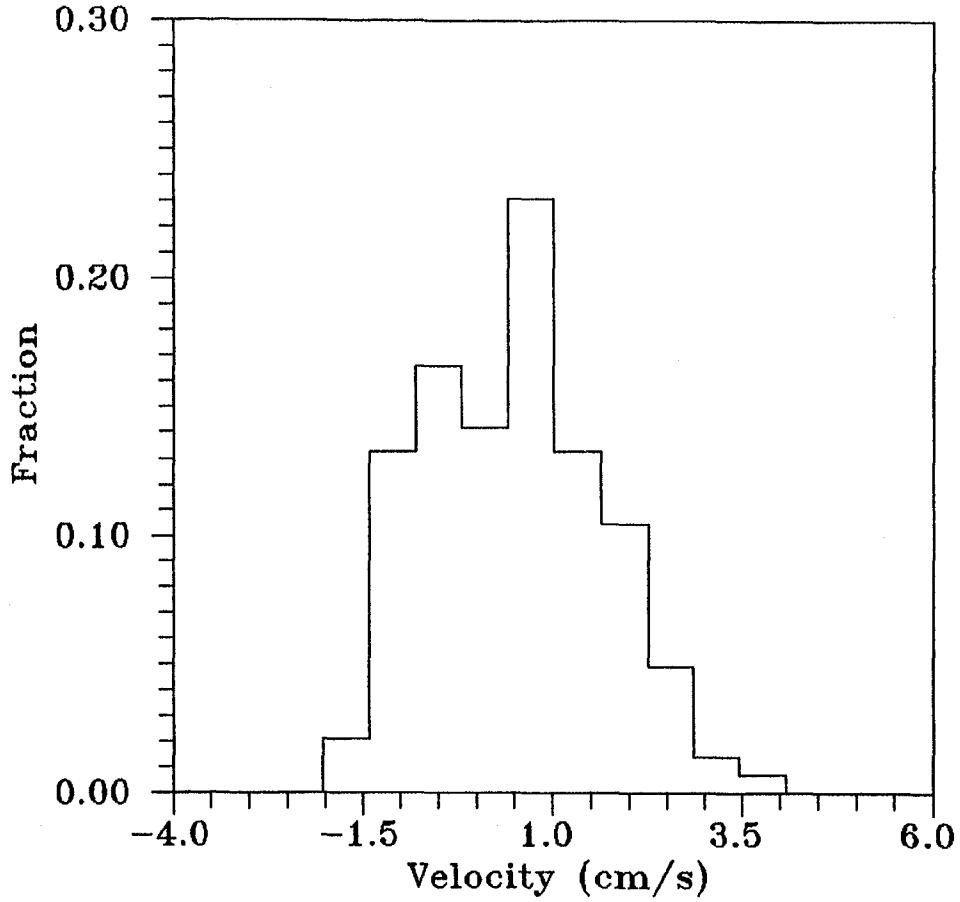

Fig. 11_a Particle Speed Distribution at Liquid Velocity=1.65 cm/s (Mean Value= 1.019cm/s, Standard Deviation=1.182cm/s)

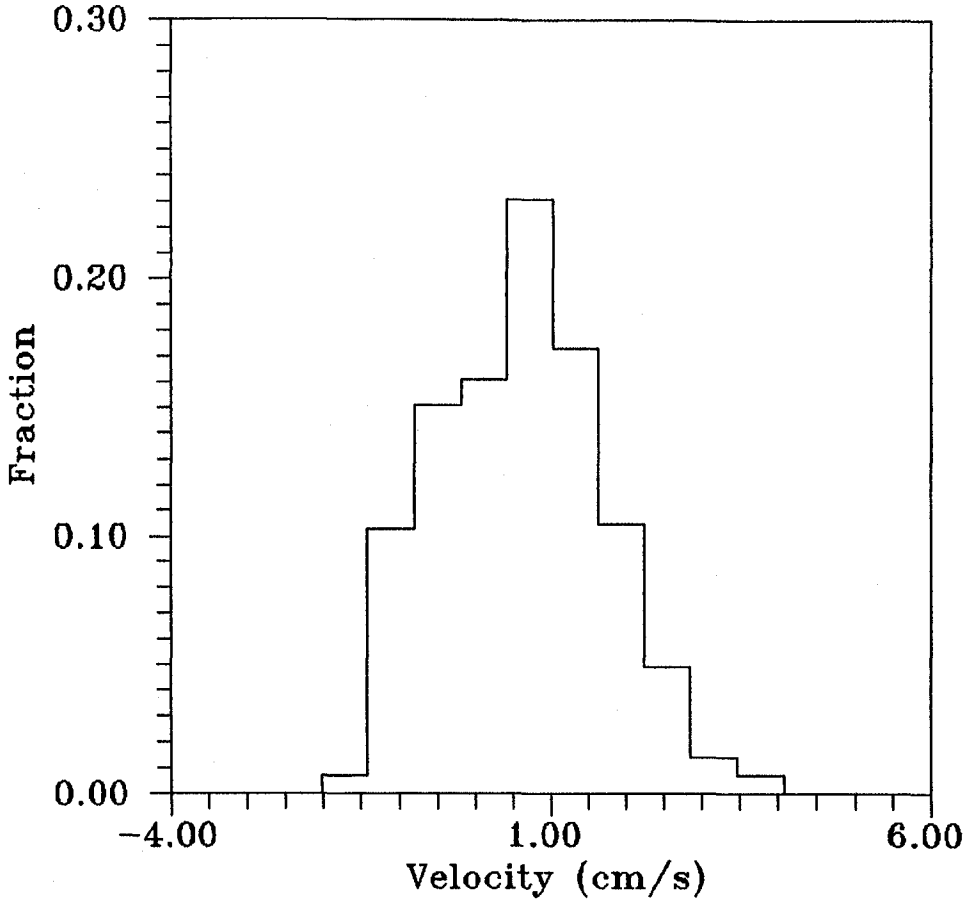

Fig. 11_b Particle Axial Velocity Distribution at Liquid Velocity=1.65 cm/s (Mean Value= 0.942cm/s, Standard Deviation=1.116cm/s)

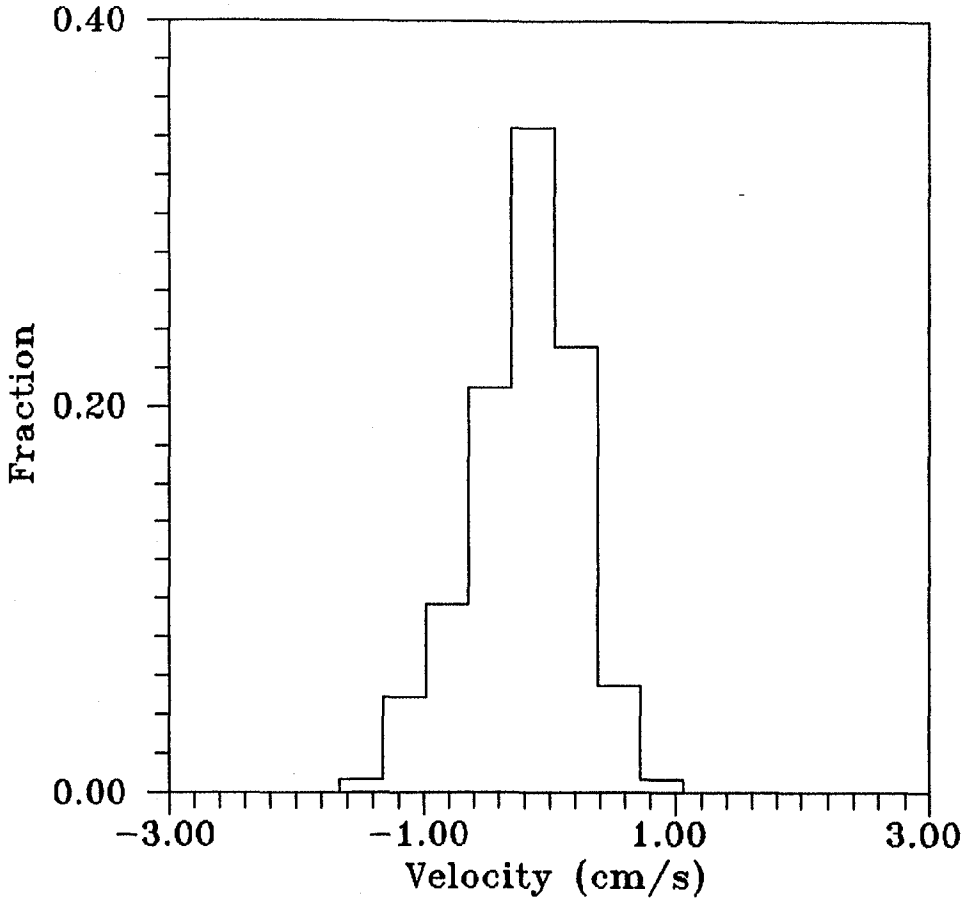

Fig. 11_c Particle Radial Velocity Distribution at Liquid Velocity=1.65 cm/s (Mean Value= 0.381cm/s, Standard Deviation=0.4811cm/s)

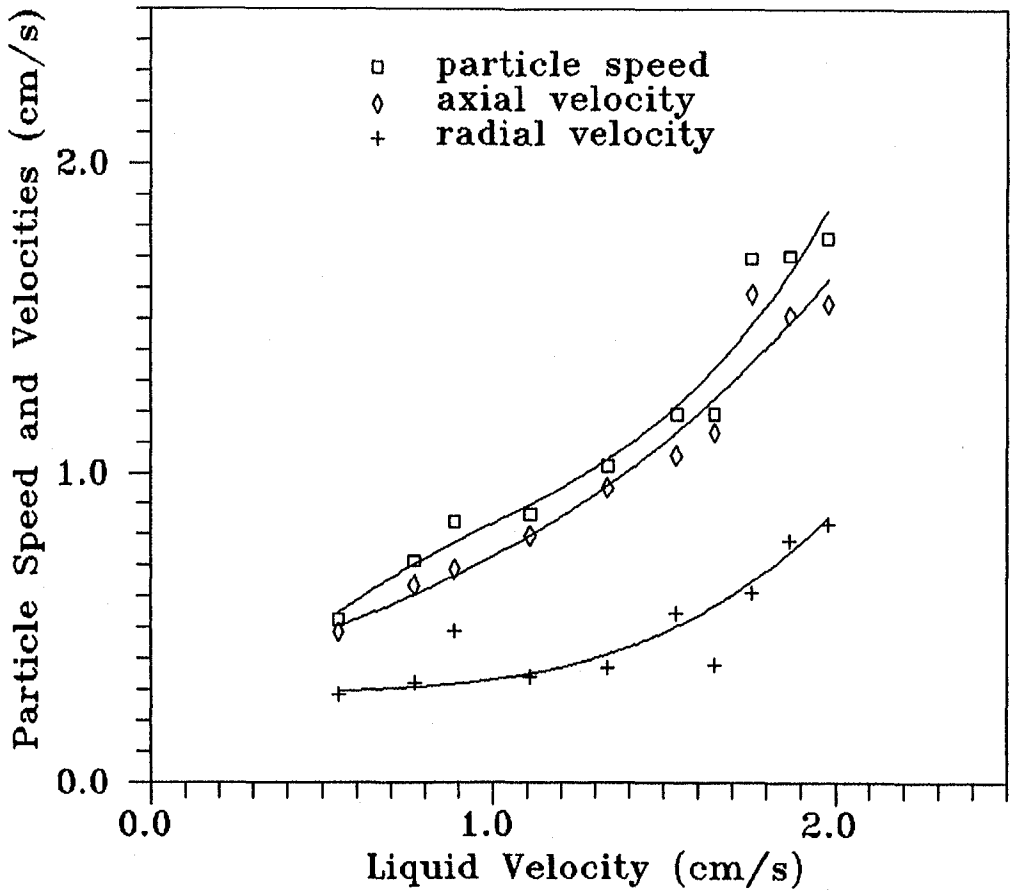

Fig. 12 Relationship Bewteen Local Average Particle Speed and Particle Velocities and The Inlet Liquid Velocities (Location: x=15.0cm, y=10.0cm, 5 mm from the wall)

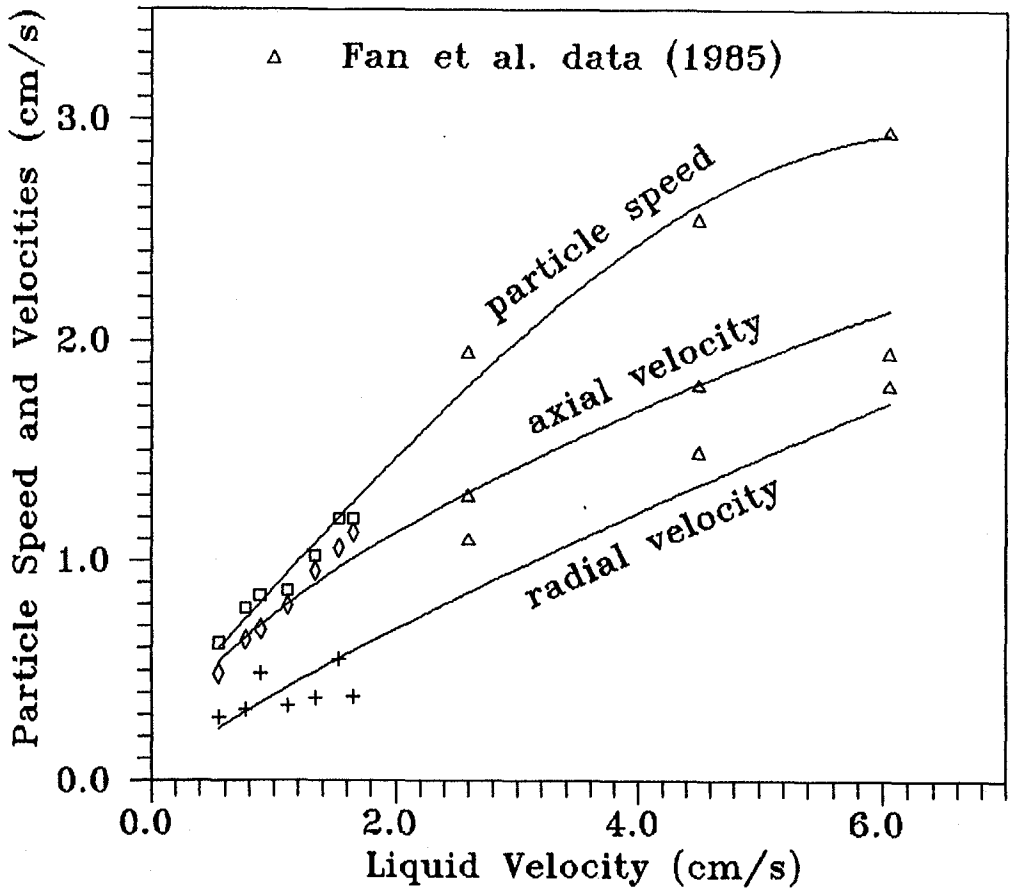

Fig. 13 Comparison of Local Average Particle Speed and Particle Velocities and The Inlet Liquid Velocities (Location:x=15.0cm, y=10.0cm, 5 mm from the wall)

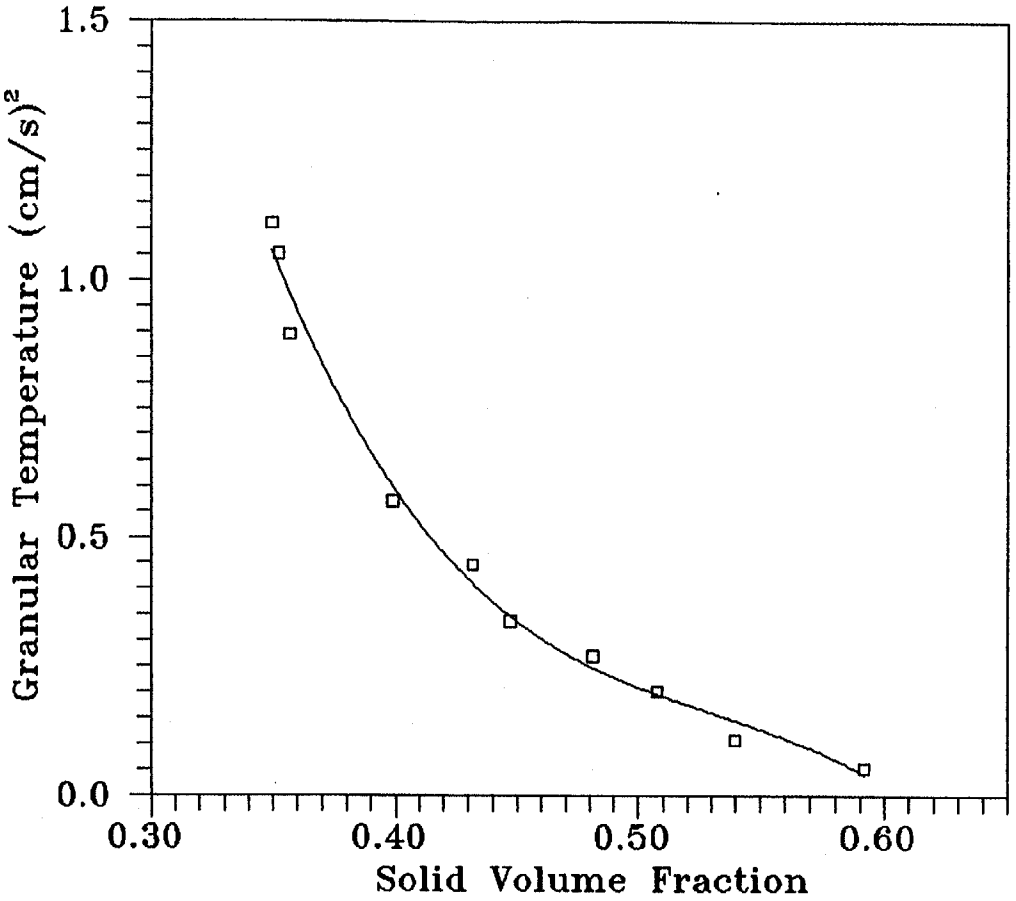

Fig. 14 Variation of Granular Temperature With Local Solid Volume Fraction For 50 Micron Catalyst Particles

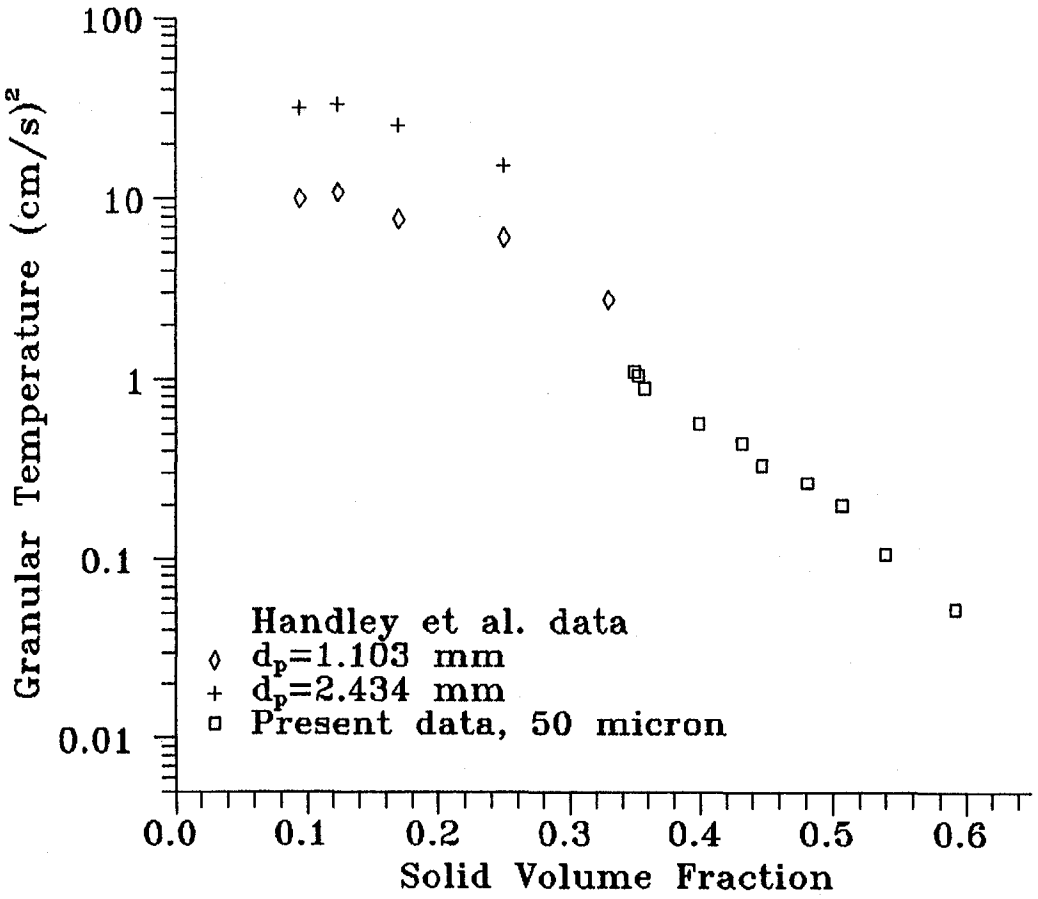

Fig. 15 A Comparison of Granular Temperature in Liquid Solid Fluidized Beds

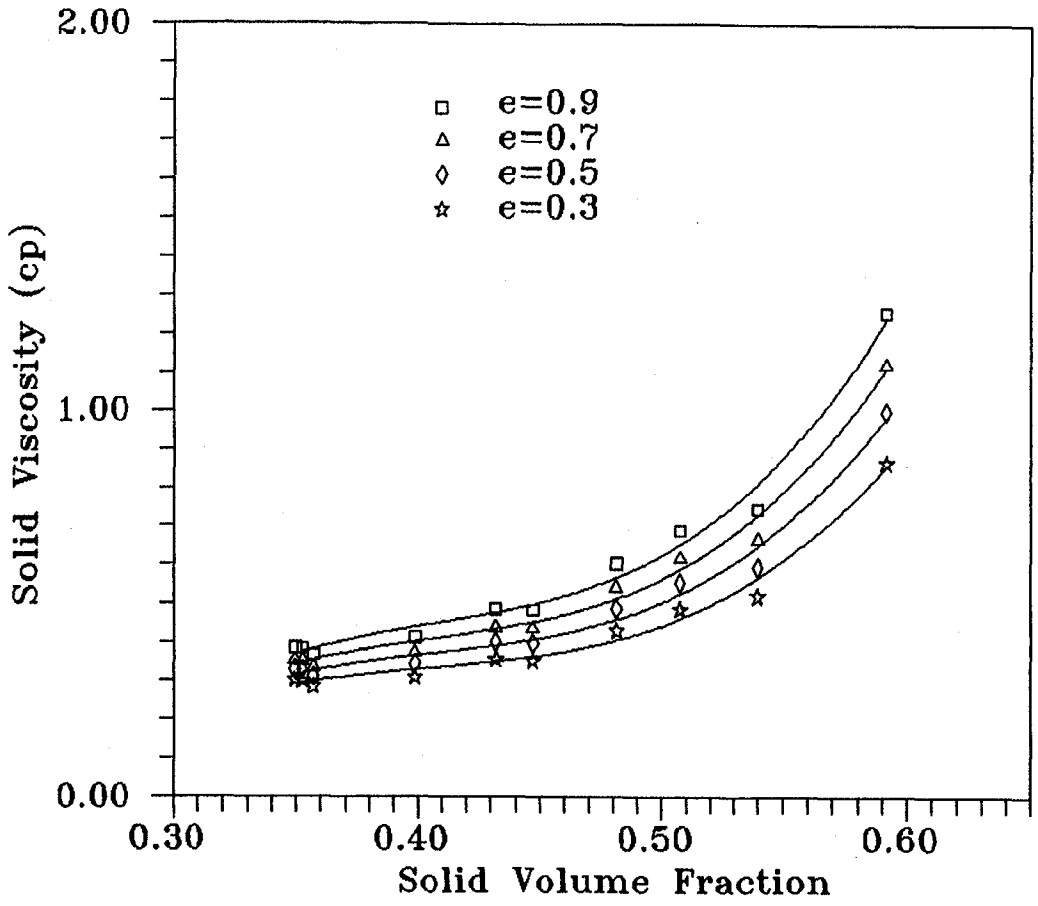

Fig. 16 Effect of Restitution Coefficient on The Collisional Solid Viscosity of 50 micron Catalyst Particles in A Water Fluid Bed

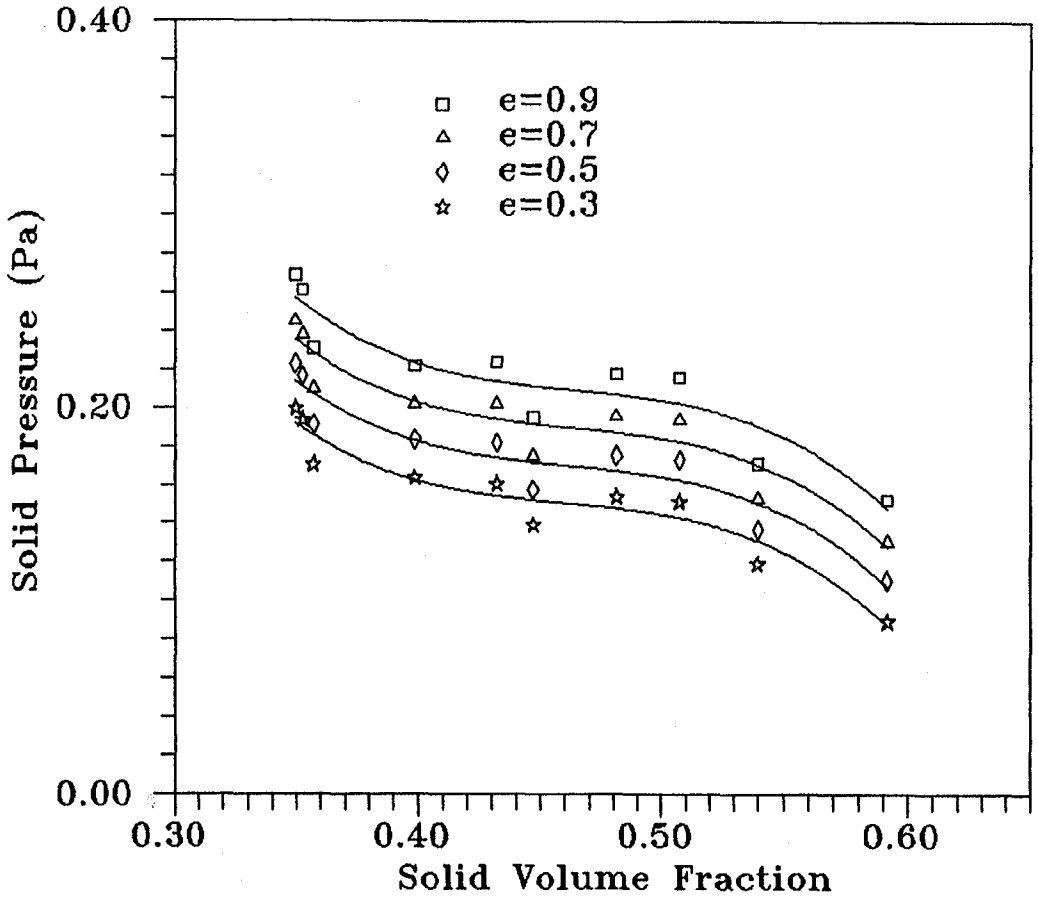

Fig. 17 Estimated Solids Pressure

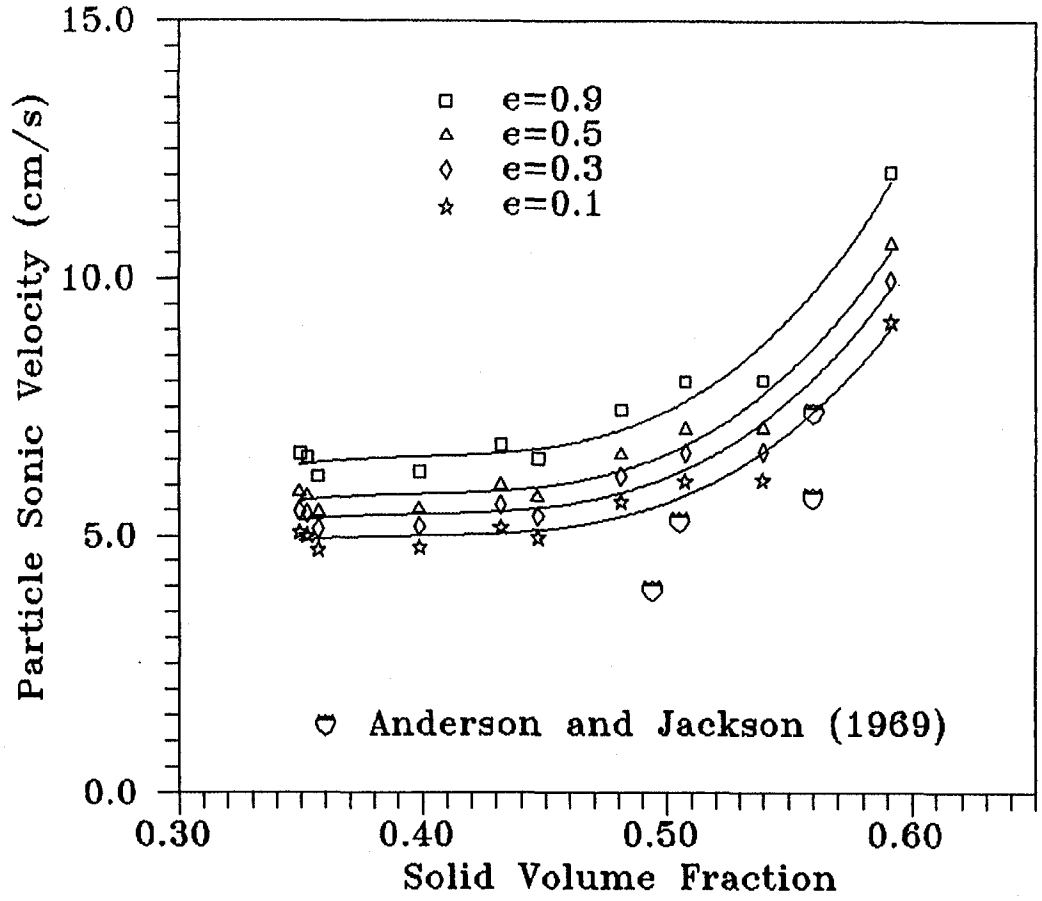

Fig. 18 A Comparison of Estimated Particle Sonic Velocity To Earlier Studies

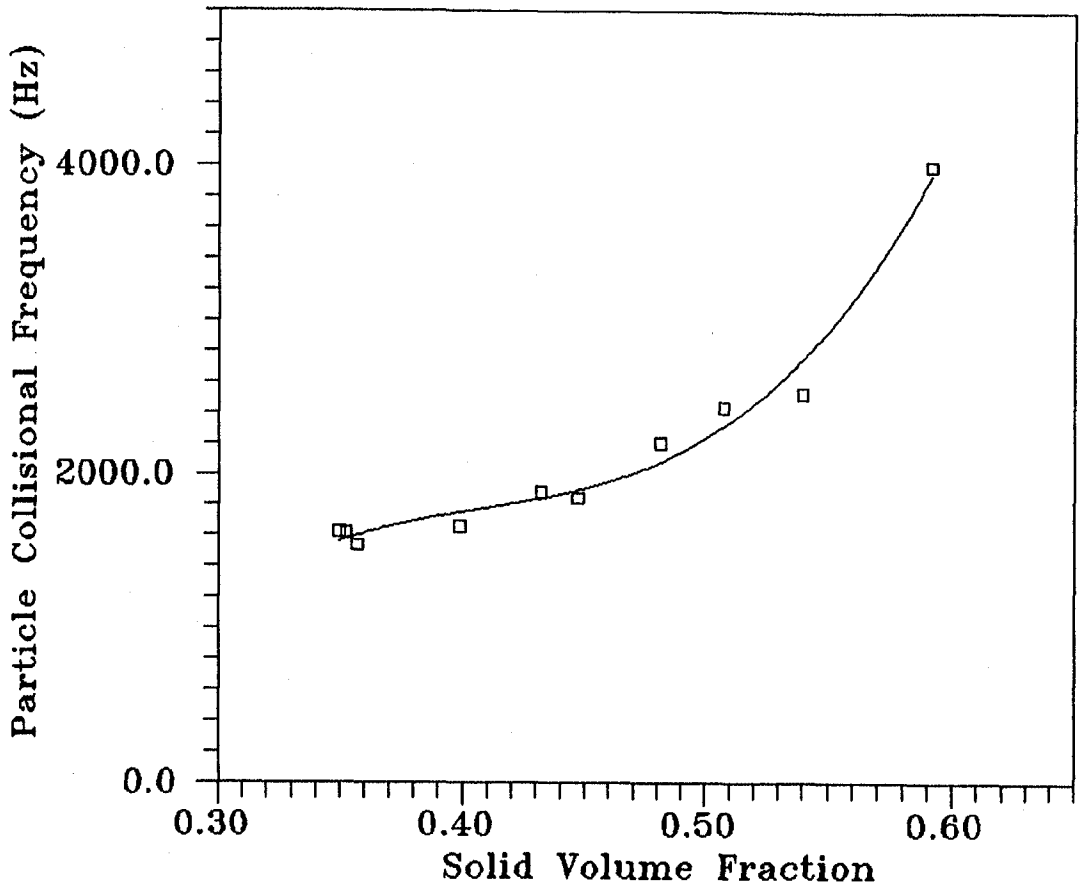

Fig. 19 Particle Collisinal Frequency For 50 Micron Catalyst Particles in A Water Fluidized Bed

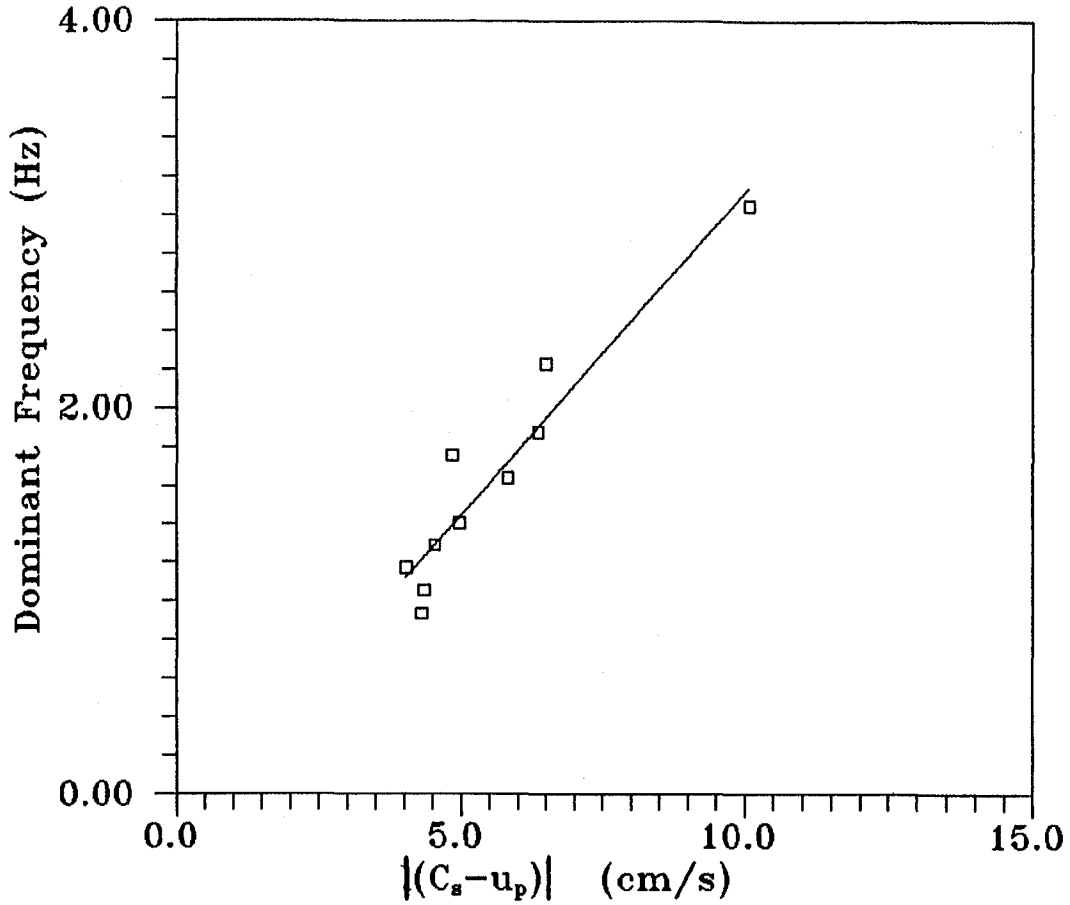

Fig. 20 A Link Between The Dominant Frequency and The Particle Path Velocity Given By Particle Sonic Velocity Minus Its Average Velocity